Investigations into oxidation induced ring opening of terarylenes containing πextended thieno[b]thiophene units

Colin Martin, Yora Goto, Ryosuke Asato, Gwénaël Rapenne, Tsuyoshi Kawai

Investigations into oxidation induced ring opening of terarylenes containing π-extended thieno[b]thiophene units

Colin J. Martin,*[a,b] Yora Goto, [a] Ryosuke Asato,[a,b] Gwénaël Rapenne[a,b,c] and Tsuyoshi Kawai *[a,b]

Four photochromic terarylenes having extended π-conjugated thieno[b]thiophene units have been prepared. Photochromic ring-cyclization and cycloreversion behaviour are exluated depending on the potision of thieno[b]thiophene units. Sponteneous fading reaction involving both thermal and cascade cycloreversion depending on molecular stucture are monitored. Electrochemical and computational studies are conducted to elucidate the relative stability of their ground and cationic states in both isomers.

Introduction

Development of new photoresponsive materials has become a key target for much biological[1,2] and materials chemistry.[3-9] The properties of photochromic diarylethenes[10,11] and terarylenes[12,13] that photochemically isomerise between open and closed forms, **O** form and **C** form, have received considerable interest in recent years. We previously reported the development of terarylene frameworks with ring cyclization quantum yields up to 98%[14] for applications including photoswitches, energy storage[15] and the generation of acids,[16-19] hydrides[20,21] and Lewis acids.[22] As part of this, we have investigated the ability of some closed form terarylenes to undergo an intermolecular radical cation exchange upon oxidation, leading to a cascade of ring cycloreversion to their **O** form. This cascade reaction proceeds with a chain reaction mechanism, in which multiple successive reactions are derived with a single activating input. However, unlike in radical[23] and ground state[24,25] chain systems, the cascade exchange occurs in the photo-generated quasi-stable state rather than the ground state. Unlike in previously described irreversible systems however,[26-28] reversible diarylethene and terarylene may offer the unique possibility that, after cascade chain propagation, the system can be reset by the application of UV light. It was first reported for diarylethenes[29] and has been studied by a number of groups.[30-38] We have reported a significantly amplified response with ring opening efficiencies up to 100,000% per oxidizing initiator (Figure 1).[37] The ring opening and closing efficiency is dependent on the delocalisation of charge on the molecule, particularly at the bridging part of the terarylene structure.[37] The mechanism first involves oxidation of the thermally stable **C** form isomer either chemically or electrochemically to the radical cationic state, $\mathbf{C}^{\cdot+}$. Then, $\mathbf{C}^{\cdot+}$ spontaneously undergoes rapid non-photochemical ring opening to the open form radical cation, $\mathbf{O}^{\cdot+}$. The $\mathbf{O}^{\cdot+}$ is reduced to the **O** form through spontaneous or cascade processes. In the cascade process, a charge transfer reaction occurs from the $\mathbf{O}^{\cdot+}$ to another **C**. This generates a stable **O** form along with a second $\mathbf{C}^{\cdot+}$ (Figure 1). This newly generated $\mathbf{C}^{\cdot+}$ will again undergo spontaneous ring opening and subsequent reduction to neutral **O** form through further generation of a radical cation $\mathbf{C}^{\cdot+}$, inducing a cascade of successive ring opening reactions. This process is thermodynamically favoured due to the energy gain upon isomerization of the **C** form to the **O** form, especially upon oxidation of the **C** with the $\mathbf{O}^{\cdot+}$.[36] The rate of spontaneous ring-opening from $\mathbf{C}^{\cdot+}$ to $\mathbf{O}^{\cdot+}$ was tuned through strategic substitution on the core of the molecule, modulating the relative stability of $\mathbf{C}^{\cdot+}$.[37]

To further design cascade active molecules, a number of factors must be considered: 1) The **C** form should be thermally stable, or quasi-stable, with a minimum number of ground state ring openings occurring to have any significant effect on the timescales of the cascade process. 2) The initial ring closing isomerisation **O**->**C** should be photochemically favourable and have a high quantum yield, Φ_{oc}, to allow for the formation of a large enough percentage of closed form in the photostationary

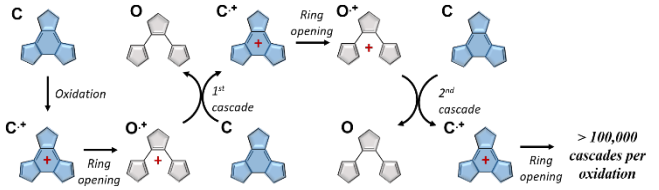

Fig. 1 Oxidative cascade ring opening and cycloreversion. Closed forms are shown in blue whereas open forms are shown in grey.

state for the cascade process to proceed. 3) The $\mathbf{O}^{\cdot+}$ and $\mathbf{C}^{\cdot+}$ radical cations should be close enough in energy to allow for a spontaneous, efficient ring opening. Previous kinetic modelling of the lifetimes has indicated that this ring opening from the radical cationic state is the rate limiting step of the cascade. 4) The overall change in energy should be thermodynamically favourable, that is to say the energy gained from the open form radical cation reverting to its neutral form ($\mathbf{E}_{\mathbf{O}\cdot+\rightarrow \mathbf{O}}$) should be larger than that lost through generation of a closed form radical cation ($\mathbf{E}_{\mathbf{C}\rightarrow \mathbf{C}\cdot+}$), such that ($\mathbf{E}_{\mathbf{O}\cdot+\rightarrow \mathbf{O}}$) – ($\mathbf{E}_{\mathbf{C}\rightarrow \mathbf{C}\cdot+}$) > 0.

We recently reported a series of highly efficient cascade terarylenes with efficiencies greater than 100,000%, optimised via changes in the steric properties of the substituents at the

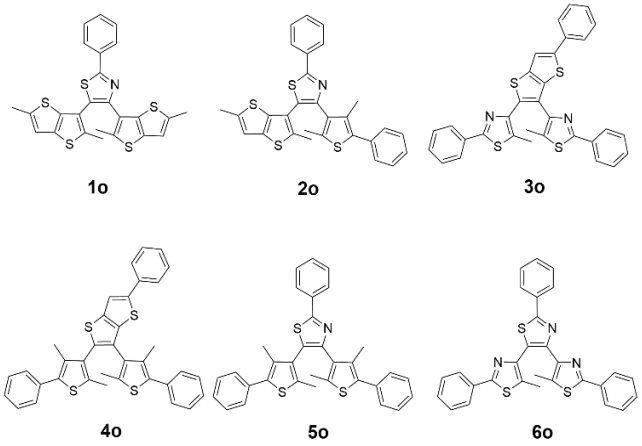

Fig. 2 Structures of compounds (open forms) discussed in this study.

position of photochromic ring formation.[37] The introduction of sterically demanding substituents at these positions was found to increase the stability of the open form and its radical cation without having a significant stabilising effect on the closed form or its radical cation. An increase in the rate of non-photochemical ring opening was observed, causing a three order of magnitude improvement in the cascade efficiency. It should be noted that the largest sterically improved cascade was a mono-phenyl substituted isomer, rather than a bis-phenyl substitution. This is due to the destabilisation of the closed form isomer upon application of too large a steric demand and a subsequent drop in the thermal lifetime of the closed form, rendering it too short lived to allow an efficient cascade. However, the effect of changes in the aromatic structure of the molecule are still nor fully understood[39,40] and how such changes will affect the rate and efficiencies of the molecular cascade remains unknown. To further examine this, we here report on attempts to further enhance the cascade through incorporation of electronically delocalised thieno[b]thiophene (TT) units as constituent parts of the terarylene frameworks. It has been proposed that the extended aromaticity of such subunits may lead to further stabilisation of the **O** and **O**$^{\cdot+}$ forms while the effect on the more conjugated **C** and **C**$^{\cdot+}$ forms will be significantly decreased. The control over this delocalisation effect was tested through incorporation of TT units into different parts of the terarylene frameworks and the resulting changes in the molecules photochemical and electrochemical properties, including their thermal and cascade stabilities, were investigated.

Results and Discussion

Molecular design and synthesis

Four target compounds **1**-**4** containing the π-delocalised TT subunit were designed (Figure 2). Each based on the existing photochromic triangle terarylene family known to undergo efficient ring cyclisation and cycloreversion upon controlled illumination. Certain members of this family are highly susceptible to cascade cycloreversion upon oxidation to their closed form radical cations. These systems will be compared to compounds **5** and **6**, the cascade activity of which have been previously described.[36] It has been shown that changes in substituents on the photochemical reaction centre carbon atoms lead to large variations in the cascade efficiency. In this study we focused not on this point and as such methyl derivatives were used in these positions in all cases. This was done as methyl substituted terarylenes are known to have good photochromic stability and will give frameworks for which the kinetics of ring opening and closing can be consistently studied.

For **1o** and **2o** the TT moiety was incorporated into the rings containing the atoms of photochromic bond formation, with a 2,7-dimethylTT fragment substituted at the 3-position, replacing the substituted thiophenes or thiazoles present in reference compounds **5o** and **6o** (Figure 2). The boronic ester intermediate 2-{2,5-dimethylthieno[3,2-b]thiophen-3-yl}-4,4,5,5-tetramethyl-1,3,2-dioxaborolane **S3**, the synthesis of which is described in the SI, was used to prepare **1o** and **2o**.

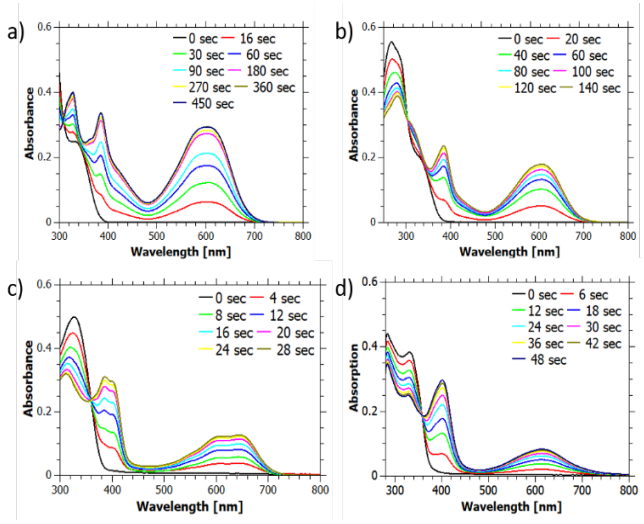

Fig. 3 New absorption bands in the visible regions of a) **1o**; b) **2o**; c) **3o** and d) **4o** upon irradiation with UV light at 365 nm in acetonitrile. Each spectrum was taken at time intervals as listed in the graph insets.

Another approach was to incorporate a TT unit as the central bridging ring. 2,3-Dibromo-7-phenyl-thieno[b]thiophene **S9**, was prepared as described in the SI and used to synthesise **3o** and **4o,** as analogues of **5o** and **6o** respectively (Figure 2). All four new compounds were fully characterised using 1D and 2D NMR with high-resolution mass spectral data (Figures S1-S12).

Photophysical investigation

The photochromic properties of **1** - **4** in acetonitrile were measured through illumination of their **O** forms at λ = 365 nm. The reversible photo-colouration and photo-bleaching behaviour is typical for the photochromic reactions of diarylethene and terarylene.[10] Characteristic isosbestic points supported 6π-ring cyclization and cycloreversion reactions. For the molecules involving TT as side units, new broad absorption bands appear with λ_{max} of 601 nm and 604 nm for **1c** and **2c**, respectively (Figure 3). For the molecules having a TT unit at the bridging position similar changes are observed, with λ_{max} of 644 nm for **3c** while **4c** displayed λ_{max} at 603 nm. The π-extended TT unit in **1c** and **2c** leads to an increase in the extinction coefficients, ε_c, of the closed forms compared to their thiophene analogue **5c**. **1c**, **2c**, **4c** and **5c** display almost similar λ_{max}, indicating minor effect of TT π-extension. **3c** shows significant bathochromic shift against **6c**. The combination of the electro-deficient thiazole rings and the electro-donative TT units seems responsible for the specific donor-acceptor (DA) character of **3c**. **1c**, **2c** and **3c** display photofading upon visible light (λ > 480 nm) irradiation, leading to the **O** form. **4o** displayed an auto-fading degradation reaction in acetonitrile, showing an unexpected increase in absorbance between 250nm and 400 nm (Figure 4a, in green).[33] Meanwhile, UV and visible light cycling of **4** in a nitrogen saturated solution, resulted in higher reversibility recovering **O** form (Figure 4b). Air-sensitive photo-degradation of **4** was also observed in chloroform within minutes, but not in toluene (Figure 4c, 4d) over the same timescale. Detailed photophysical analysis in acetonitrile were carried out for all compounds (Table 1). All these compounds

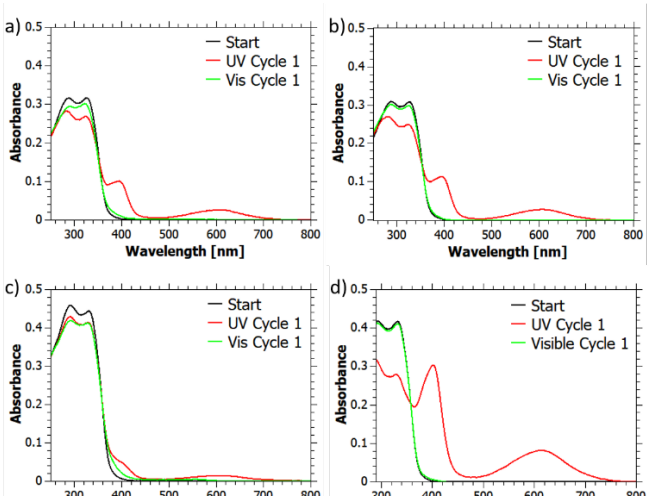

Fig. 4 Changes in absorption of **4o** upon irradiation with UV light at 365 nm in a) acetonitrile under air; b) acetonitrile under nitrogen; c) chloroform under air and d) toluene under air.

displayed Φ_{oc} between 45 and 74% and Φ_{co} between 1.8 and 2.2%. The higher Φ_{oc} of **3** is attributable to the effect of intramolecular S-N interactions stabilizing the reactive conformation.[14] These Φ_{oc} and Φ_{co} are similar to the reference compounds and other photochromic terarylenes and the TT unit seems to have no marked impact on the photochemical cyclization and cycloreversion pathway. [12-14]

Table 1 Optical properties and photochemical quantum yield of compounds 1-6 [a)]

	ε_O $dm^3 \cdot mol^{-1} \cdot cm^{-1}$ (λ_{max})	ε_C $dm^3 \cdot mol^{-1} \cdot cm^{-1}$ (λ_{max})	Φ_{oc}	Φ_{co}
1	34,700 (272 nm)	13,500 (601 nm)	45 %	1.9 %
2	29,700 (267 nm)	13,500 (604 nm)	64 %	2.2 %
3	44,200 (327 nm)	11,800 (644 nm)	74 %	1.8 %
4	35,000 (326 nm)	n.a. (603 nm)	n.a.	n.a.
5[b)]	35,000 (269 nm)	9,400 (610 nm)	60 %	7.0 %
6[b)]	31,500 (315 nm)	16,000 (587 nm)	40 %	3.0 %

a) in acetonitrile, b) from ref. 12

Electrochemical investigation

We then assessed the suitability of the compounds towards the radical cation formation necessary for cascade cycloreversion to proceed. Cyclic voltammetry of compounds **1**–**4** and **6** were measured in $1x10^{-3}$ M acetonitrile solution referenced to Fc/Fc^+ containing 0.1 M $TBAPF_6$ as electrolyte. A summary of oxidation potentials is shown in Table 2 and compared the values previously reported for **5** and **6**.[36] The open form isomers all showed a single or double irreversible oxidation with onsets between +0.68 and +0.83 V (Figure 5, left). These irreversible oxidations all have maximums greater than +0.78 V (vs Fc/Fc^+) and are similar to those reported for open-ring isomers of diarylethenes and terarylenes.[29,33] Due to the electron donating effect of the TT unit at the bridging position in **3o** and **4o** the first oxidation is seen at a slightly lower potential compared to **1o** and **2o** and reference compounds **5o** and **6o**. Each compound was then dissolved in 3 mL of toluene and illuminated using UV light (λ = 365 nm) for ninety minutes to generate photostationary states (**PSS**) containing a majority of closed form isomers. The solvent was removed under reduced pressure and the coloured solid obtained redissolved in a 0.1 M $TBAPF_6$ acetonitrile solution and the voltammetry of the **PSS** measured *vs.* Fc/Fc^+, from which the oxidation peaks of the closed form can be observed.

Table 3 DFT calculated energy differences between the different forms of **1 – 6** [a)]

	1	**2**	**3**	**4**	**5**	**6**
ΔE_{C-O}	51.9	67.6	59.2	100.2	80.2	68.6
$\Delta E_{C^{\cdot+}-C}$	543.1	542.7	558.4	521.0	538.2	574.4
$\Delta E_{O^{\cdot+}-O}$	633.5	635.1	619.6	626.6	637.9	648.0
$(\Delta E_{O^{\cdot+}-O}) - (\Delta E_{C^{\cdot+}-C})$	90.3	92.4	61.2	105.6	99.7	73.6
$\Delta E_{C^{\cdot+}-O^{\cdot+}}$	-38.4	-24.8	-2.0	-5.4	-19.4	-4.9

a) in kJ mol^{-1}.

Table 2 Electrochemical oxidation potential of compounds **1 – 6**[a)]

	E_{onset}^{open}	E_{peak}^{open}	E_{onset}^{PSS}	E_{peak}^{PSS}	ΔE_{onset}^{O-C} = E_{onset}^{open} - E_{onset}^{PSS}
1	0.73	0.80, 0.83	-0.10	-0.03, 0.18, 0.82	0.83
2	0.78	0.85, 1.03	-0.09	-0.03, 0.18, 0.93	0.87
3	0.74	0.78, 0.91	0.14	0.20, 0.48, 0.94	0.60
4	0.68	0.79	-	-	-
5[36]	0.83	0.87, 1.12	-0.19	-0.04, 0.87, 1.09	1.02
6[36]	0.80	0.92, 1.12	-0.09	-0.01, 0.89, 1.14	0.89

a) in a $1X10^{-3}$ M acetonitrile solution containing 0.1 M TBAPF, potential is given in V *vs.* Fc/Fc^+

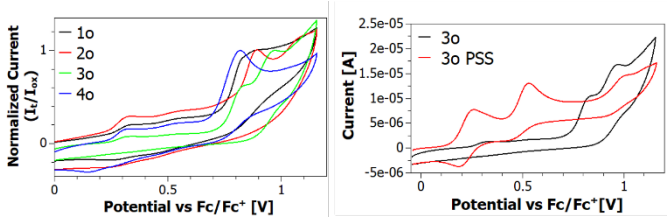

Fig. 5 Cyclic voltammograms of **1o**-**4o** (left, normalised relative to the first oxidation maximum) and **3o** and $\mathbf{3}_{PSS}$ (right). Measurements were performed in acetonitrile ($1x10^{-3}$ M; **PSS** generated from $1x10^{-3}$ M solutions of the **O** form) using $TBAPF_6$ (0.1 M) as the electrolyte.

For $\mathbf{1}_{PSS}$, $\mathbf{2}_{PSS}$ and $\mathbf{3}_{PSS}$, two successive semi-reversible oxidation peaks are seen in the region between -0.03 and +0.48 V along with a third irreversible oxidation in the same region as the first oxidation of the respective **O** form. In the case $\mathbf{4}_{PSS}$ a very fast electrochemically induced ring opening upon application of even a small potential is observed, leading to decolouration, almost immediately upon initiation of voltammetry scans. It appears that this system undergoes fast ring opening upon generation of the closed form radical cation and as such its electrochemical profile could not be measured. The oxidations observed for $\mathbf{1}_{PSS}$, $\mathbf{2}_{PSS}$ and $\mathbf{3}_{PSS}$ represent their first and second oxidised radicals which immediately induce cascade ring opening; as such their voltametric signals are often weak.[29] Weak oxidation waves are seen for $\mathbf{1}_{PSS}$ and $\mathbf{2}_{PSS}$ while for $\mathbf{3}_{PSS}$ clear quasi-reversible oxidations are observed (Figure 5, right). Indeed, the intensity of the first and second oxidations observed in $\mathbf{3}_{PSS}$ (Figure 5, right) also infers it has a more stable closed form radical, $\mathbf{C}^{\cdot+}$, which may affect its cascade reactivity. In all cases the presence of a third oxidation above +0.8 V is consistent with previous reports in which some electrochemical ring opening to the **O** form is observed in conjunction with the presence of residual **O** form in the **PSS**.[36]

The driving force of the cascade reaction is given by the reduction of $\mathbf{O}^{\cdot+}$ form to **O** form through the regeneration of a new $\mathbf{C}^{\cdot+}$. As such it is the relative oxidation potentials of the neutral open and closed forms ($\mathbf{E_{ox}^{open}}$ vs. $\mathbf{E_{ox}^{closed}}$), rather than their relative energy levels, that indicate if a terarylene will be susceptible to the cascade reaction. Whereby if the first oxidation potential of the open form to its radical cation is greater than that of the closed form to its radical cation ($\mathbf{E_{ox}^{open}} > \mathbf{E_{ox}^{closed}}$), the cascade reaction seems favourable. For **1**, **2** and **3**, the open form requires a higher applied potential than the closed one to be oxidised (Table 2), indicating that the electron transfer required during the cascade process is favourable in all cases.

DFT studies

To give further understanding of these substances susceptibilities towards cascade reactivity, the open, closed, and radical cation forms of each were calculated via Gaussian DFT[41] using the B3LYP Model and the 6-31+G(d,p) basis set. The free energy of each molecule in the four states (**C**, $\mathbf{C}^{\cdot+}$, **O** and $\mathbf{O}^{\cdot+}$) were computed and the differences calculated following zero-point correction as described by Irie[42] (Table 3 and Figure 6). For all substances, large positive values of $\mathbf{\Delta E_{C-O}}$ imply the thermodynamic stability of **O** forms compared to their corresponding **C** form, possibly because of aromatic stabilization of the **O** forms. $\mathbf{\Delta E_{O^{\cdot+}-O}}$ values are all larger than $\mathbf{\Delta E_{C^{\cdot+}-C}}$ and positive values for the total energy change ($\mathbf{\Delta E_{O^{\cdot+}-O}}$) - ($\mathbf{\Delta E_{C^{\cdot+}-C}}$) were elucidated for all compounds. This supported

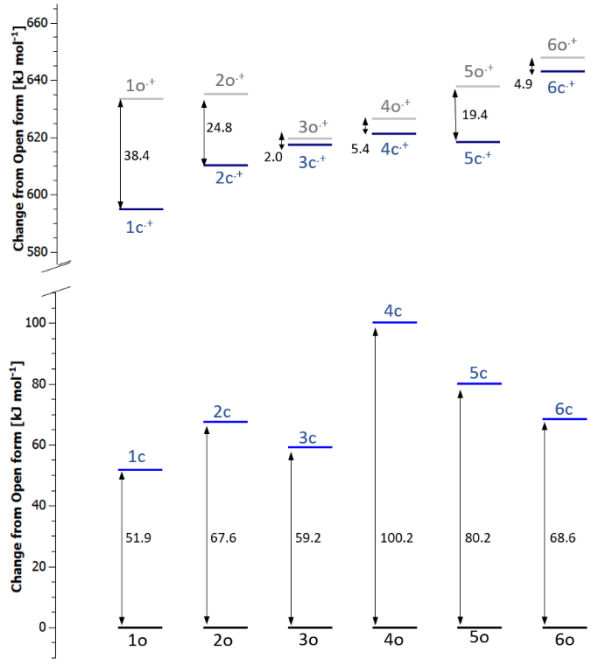

Fig. 6 Schematic of the relative energy differences, $\mathbf{\Delta E_{C-O}}$ and $\mathbf{\Delta E_{C^{\cdot+}-O^{\cdot+}}}$ (kJ. mol^{-1}), in the neutral and radical cationic states.

the lower oxidation potential of **C** form than **O** form and thermodynamically favourable cascade reaction (Table 3, $\mathbf{\Delta E_{O^{\cdot+}-O}} > \mathbf{\Delta E_{C^{\cdot+}-C}}$) for all compounds.

For **1** and **2**, the energy difference of $\mathbf{C}^{\cdot+}$ and $\mathbf{O}^{\cdot+}$, $\mathbf{\Delta E_{C^{\cdot+}-O^{\cdot+}}}$ indicates the more thermodynamically stable $\mathbf{C}^{\cdot+}$ form ($\mathbf{\Delta E_{C^{\cdot+}-O^{\cdot+}}} < 0$) and a less favourable cascade ring opening reaction, as described by Irie et al.[42] For **3** and **4**, $\mathbf{C}^{\cdot+}$ and $\mathbf{O}^{\cdot+}$ are much closer in energy ($\mathbf{\Delta E_{C^{\cdot+}-O^{\cdot+}}} \sim 0$). It has been shown that in cascade reactivity the rate limiting step is the non-photochemical isomerization from the $\mathbf{C}^{\cdot+}$ to the $\mathbf{O}^{\cdot+}$ form and that the reaction is driven by the total energy change on converting $\mathbf{O}^{\cdot+}$ to **O** and **C** to $\mathbf{C}^{\cdot+}$ as each step of the cascade proceeds. These calculations also show the effect of the TT fragment. The TT units at the side of compounds **1** and **2** seem to promote significantly negative $\mathbf{\Delta E_{C^{\cdot+}-O^{\cdot+}}}$, which is especially remarkable in **1** with two TT units present. $\mathbf{\Delta E_{C^{\cdot+}-O^{\cdot+}}}$ of **2** is also lower compared to **5**, suggesting again the suppressing effect of TT units on the cascade reactivity. Interestingly, we observed the opposite effect for the TT unit at the central bridging unit. That is, $\mathbf{\Delta E_{C^{\cdot+}-O^{\cdot+}}}$ of **3** and **4** with a TT bridging unit were less negative than the corresponding substances, **6** and **5**, respectively. This promotes the relative stability of the $\mathbf{O}^{\cdot+}$ forms of **3** and **4** and a facile cascade ring-opening reaction.

Cycloreversion properties

To further test the suitability of these systems for the cascade reaction, their **C** form thermal stabilities were measured. In each case a PSS solution containing a majority **C** form isomer was generated through illumination of the **O** form with UV light (typically 2 min for $\mathbf{1}_{PSS}$, $\mathbf{2}_{PSS}$ and $\mathbf{3}_{PSS}$ and 30 sec for $\mathbf{4}_{PSS}$) and then the absorption at the wavelength maximum of **C** form was measured over time (Figure 7).

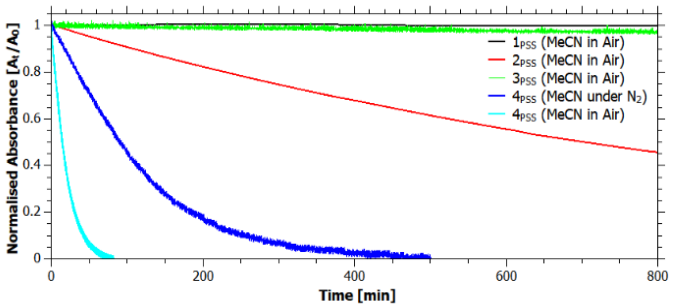

Fig. 7 Thermal decay in absorbance at λ_{max} of **PSS** solutions of **1**-**4** in acetonitrile.

For **1** and **3** this resulted in the formation of a long-lived **PSS** with slow decay of the **C** forms. This went in a first order manner with half lifetimes of 178 days for **1c** and 302 hours (12.6 days) for **3c**, such values are typical for terarylenes in which the ring opening cycloreversion is photoinitiated (P-type) with visible light (Table 4). For $\mathbf{2}_{PSS}$, however, we observed a significantly shorter lifetime of 11.8 hours, also obeying first order kinetics. The speeding up of the cycloreversion indicates $\mathbf{2}_{PSS}$ behaves as a partly combined system of both thermal (T-type) and light activated (P-type) processes. This short lifetime of **2c** in comparison with **1c** and **3c** should be attributable to a steric effect with the 4-methyl unit in the side phenyl-thiophene group in **2c**. In other words, we expect specific intramolecular S-N tethering interactions stabilise **1c** and **3c**.

For $\mathbf{4}_{PSS}$, rapid fading of the closed form is seen in both aerated and deaerated solutions with decays an order of magnitude faster than **1** and **3** (Figure 7). The non-first order decay of $\mathbf{4}_{PSS}$ in acetonitrile suggests some additional processes, possibly spontaneous cascade reactions. In toluene solution (Figure S13) a first order decay with a lifetime of 8.9 hours was observed for $\mathbf{4}_{PSS}$. In comparison between **4** and **5**, the central TT bridge unit in **4** seems to increase the energy difference between **C** form and **O** form as seen in Table 3 and an enhancement in the thermal decay kinetics of **4c**. However, this trend was opposite for **3** and **6**. Currently we do not have appropriate explanation and capable prediction of the effect of TT since there may be a complicated combination of steric and thermodynamic effects.[15]

We also assessed here the spontaneous fading after UV light irradiation in a mixed solution system. For some applications of the cascade reactivity, including UV and X-Ray detection, halogenated solvents are required due to photo-oxidizing effect and stability of the radical cations involved.[33] 0.3 mL solutions of **1o**-**4o** in toluene were illuminated (λ = 365 nm) until a concentration of the **C** form became 9.0×10^{-8} M. Then, the solution was diluted with 2.7 mL of chloroform, giving a 9:1 chloroform: toluene solution of closed form (concentration = 3.0×10^{-5} M) and their spontaneous fading stability was monitored (Figure S14). As with the acetonitrile case $\mathbf{4}_{PSS}$ showed a much faster, non-first order cycloreversion in 9:1 chloroform: toluene compared to **1**-**3**, with full ring opening seen within 15 min, indicating a high susceptibility to cascade processes. This rapid increase in ring opening time on switching solvents indicates the halogenated solvent assists in the cascade reactivity. To observe if this ring opening rate change can also be induced by UV light, a solution of $\mathbf{4}_{PSS}$ in 9:1 chloroform: toluene was then irradiated with a controlled number of photons (λ = 365 nm) and the decay compared to that of an unilluminated solution (Figure 8). This decay was sped up, reaching complete decolouration within 1,800 seconds an increase from the 7,500 sec needed for the non-illuminated solution and indicating the successful initiation of the cascade ring opening via short UV excitation.

We then studied the cascade reaction of **1c**-**3c** using tris(bromophenyl) ammoniumyl hexachloroantimonate (TBPA) as a one electron oxidizing initiator. Formation of the radical cation $\mathbf{C}^{\cdot+}$ is expected to induce the cascade ring opening. For **2** and **3**, addition of 0.1 equivalents of TBPA to an acetonitrile

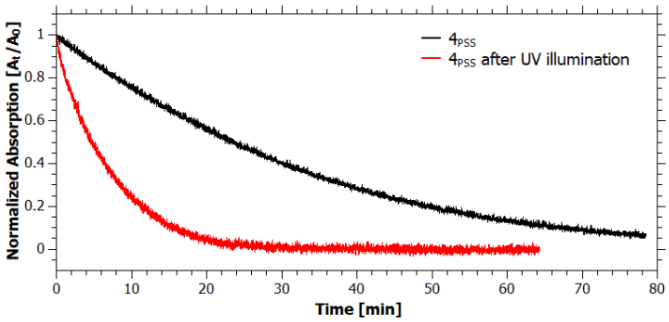

Fig. 8 Decay in absorbance at λ_{max} $\mathbf{4}_{PSS}$ in 1:9 chloroform: toluene with and without UV irradiation (365 nm).

Table 4 Rate constants and lifetimes of thermal decay

	First order rate constant of thermal decay	Lifetime of thermal decay
1c[a)]	4.50×10^{-8} s^{-1}	178 days
2c[a)]	1.63×10^{-5} s^{-1}	11.8 hours
3c[a)]	6.37×10^{-7} s^{-1}	302 hours
4c[b)]	2.17×10^{-5} s^{-1}	8.9 hours
5c[c)]	~3×10^{-8} s^{-1}	14 days
6c[c)]	~9.5×10^{-9} s^{-1}	3.3 years

a) in acetonitrile, b) in toluene, c) from ref 12

solution of the **PSS**, resulted in ring opening faster than seen thermally (Figure 9). For **2**, the cascade leads to a rapid increase in cycloreversion rate, competed within 22 minutes, compared to a half-life of 11.8 hours thermally (Figure 9). Also, a big enhancement is seen for **3**, going from a thermal half-life of 302 hours to completion within 8 hours upon addition of TBPA (Figure 9, inset). For $\mathbf{1_{PSS}}$, the rate of closed form decay remained unchanged from that observed thermally which is consistent with the higher energy difference between **C**$^{\cdot+}$ and **O**$^{\cdot+}$ forms predicted by DFT calculations ($\Delta E_{C^{\cdot+}-O^{\cdot+}}$, Table 3 and Figure 6).

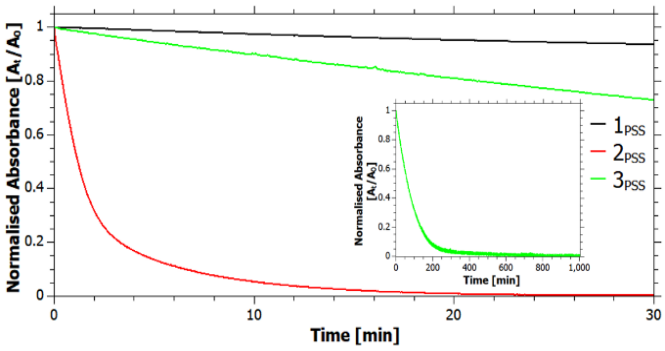

Fig. 9 Decay in absorbance at λ_{max} of PSS solutions of **1**-**3** in acetonitrile upon addition of 0.1 eq. of TBPA; inset extended timescale for $\mathbf{3_{PSS}}$.

Kinetic study of 4

As **4** is susceptible to cascade reactivity while also undergoes thermal cycloreversion with a lifetime in the scale of hours in acetonitrile, it offers an excellent platform to model the kinetics of cycloreversion reactivity. Its thermal ring opening can, unlike the longer-lived examples **1**-**3** and **5**-**6**, be modelled in terms of overlapping cascade and thermal ring opening mechanisms with its thermal decay appearing as a non-first-order mixture of both processes. In toluene (Figure S13), the absorption decay of $\mathbf{4_{PSS}}$ occurs in an exponential, first order manner, attributed only to reversible ring opening. This indicates that in acetonitrile the deviation from first order kinetics comes from other ring opening processes, possibly induced by ambient radiation triggering some formation of the **C**$^{\cdot+}$ radical cation and initiation of cascade. The decay in acetonitrile under nitrogen was modelled in terms of the ratio of the initial concentration of the closed form to its radical cation ([**C**$^{\cdot+}$]:[**C**]) as well as six kinetic parameters (Figure 10, k_1-k_6). The rates of reversible ambient exchange between the **C** and **C**$^{\cdot+}$ states are defined as k_1 and k_6, and the rates of spontaneous thermal ring opening of **C**$^{\cdot+}$ to **O**$^{\cdot+}$ and **C** to **O** are defined as k_2 and k_5 respectively (Figure 10). Along with this, the decay of **O**$^{\cdot+}$, through reduction to neutral **O** without (k_3) or with reformation of **C**$^{\cdot+}$ through the cascade process (k_4) were also defined. It can be assumed that the

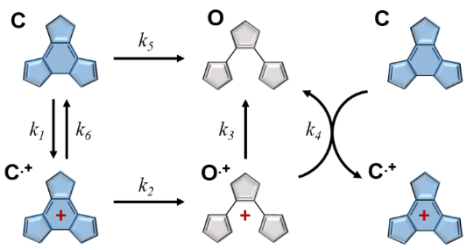

Fig. 10 Reactive species and rate constants in the ring opening of **4c**. Closed forms are shown in blue whereas open forms are shown in grey.

timescales of each of these processes are different and that the rates come in the order $k_4 >> k_2$, k_3, $k_5 > k_1$, k_6. This leaves the rate equations for the concentrations of each species in solution as shown in Figure 11. On the timescales of hours involved in the thermal cycloreversion of **4**, the dark thermal exchanges between **C** and **C**$^{\cdot+}$ are negligible (k_1, k_6) and can be assumed to be ~0. Based on previous reports[32] a value for k_5 can be calculated from the thermal decay of the toluene solution of **4c** (Figure S13) where no cascade takes place and was found to be 2.17×10^{-5} s^{-1}. Then to an acetonitrile solution of $\mathbf{4_{PSS}}$ in a nitrogen atmosphere, 1 equivalent of the single electron oxidant TBPA was added and the decolouration of this 100% **C**$^{\cdot+}$ solution measured as it spontaneously ring opened (Figure S15). Fitting this to a first order decay gave a value for k_2 of 5.21×10^{-3} s^{-1}. Similar measurements for **5** and **6** showed radical cation decay rates of 1.07×10^{-2} s^{-1} and of 3.75×10^{-2} s^{-1} respectively. Using these parameters, the experimentally measured decay of $\mathbf{4_{PSS}}$ in acetonitrile under a nitrogen atmosphere was modelled for fitting values of k_3 and k_4; the results are shown in Table 5 and Figure S16 and compared to those of reference compound **6** previously measured via stop flow methods.[12]

$$\frac{d[C]}{dt} = -k_1[C] - k_4[C][O^{+\cdot}] - k_5[C] + k_6[C^{+}]$$

$$\frac{d[C^{+\cdot}]}{dt} = k_1[C] - k_2[C^{+\cdot}] + k_4[C][O^{+\cdot}] - k_6[C^{+}]$$

$$\frac{d[O^{+\cdot}]}{dt} = k_2[C^{+\cdot}] - k_3[O^{+\cdot}] - k_4[C][O^{+\cdot}]$$

$$\frac{d[O]}{dt} = k_3[O^{+\cdot}] + k_4[C][O^{+\cdot}] + k_5[C]$$

Fig. 11 Kinetic equations for the changes in concentrations of each form of **4** when undergoing the cascade cycloreversion

For **4**, a decrease in the rate of spontaneous ring opening of the closed form radical cation (k_2) compared to the reference compounds is seen. This can be attributed to the changes in the relative stabilities due to the TT unit as seen in the DFT calculations, with the slower radical cation ring opening of the

Table 5 Fitted kinetic parameters for the cascade cycloreversion of **4**, **5** and **6**

	k_1 (s^{-1})	k_2 (s^{-1})	k_3 (s^{-1})	k_4(s^{-1})	k_5(s^{-1})	k_6 (s^{-1})	[C$^{\cdot+}$]:[C]
4	-	5.21×10^{-3}	6.57×10^{-5}	2.37×10^{3}	2.17×10^{-5}	-	1:41
5	-	1.07×10^{-2}	-	-	months		
6	-	3.75×10^{-2}	3.0×10^{-2}	2×10^{4}	years	-	-

C$^{\cdot+}$ resulting from the changes in the relative stabilities of its **O**$^{\cdot+}$ and **C**$^{\cdot+}$ forms. Particularly of note is the strongly enhanced stability seen in the open form radical cation **O**$^{\cdot+}$ of **4**, with a three order of magnitude decrease in its non-cascade decay (k_3) and a subsequent increase in the lifetime of the **O**$^{\cdot+}$ radical cation compared to **6**. However, a less significant change is observed in the rate of cascade exchange k_4 which falls by one order of magnitude. Indeed, it appears the major factor that is affecting the ring opening of **4c** is the increased stability of the open form radical cation **O**$^{\cdot+}$ induced by the presence of the π-delocalised bridging TT subunit. This infers that a higher concentration of **O**$^{\cdot+}$ is present in solution, increasing the rate of cascade reaction. From the fitting, an extrapolation of the initial ratio of the closed isomer and its radical cation [**C**$^{\cdot+}$]:[**C**] in solution was performed, with forty one closed forms present for each radical cation. The source of these radial cations in solution remains unknown but may possibly result from ambient background radiation leading to some formation in nitrogenated acetonitrile.

By using these values (k_1-k_6), the decay of **4o** in aerated acetonitrile was then fitted to estimate the change in the ratio of [**C**$^{\cdot+}$]:[**C**] resulting from the presence or absence of air in the solution. From this, the increased decay rate in aerated acetonitrile was seen to result from an increase in the ratio of [**C**$^{\cdot+}$]:[**C**] from 1:41 to 1:3.9 again as with in the case of chloroform indicting that some ambient effects from either oxygen or ambient radiation can trigger the cascade ring opening of **4c**.

Conclusions

We have developed a series of photochromic terarylenes containing extended π-aromaticity through incorporation of TT subunits into their molecular core. Systematic photochemical, electrochemical and computational analysis shows how changes in the nature of the ground and radical cationic states of the photochromic isomers of each structure can affect their susceptibility towards ring opening cascade processes. In particular tuning the π-conjugation at the bridging part of the triangle terarylene allows for control over the molecules ring opening kinetics, through stabilisation and destabilisation of the closed form ground and radical cationic states. Four new photochromes each showing highly efficient cycloreversion properties have been prepared and characterised with photophysical and electrochemical studies allowing for comparison with existing reference compounds. For key compound **4**, the favourable timescales of thermal and cascade ring opening in acetonitrile allowed for detailed modelling of its cycloreversion kinetics. This has led to further details into the nature of the cascade mechanism and how it can be tuned through destabilisation of the radical cation of the closed form photochrome. This, in conjugation with previous reports on changes in the substitution patterns at other parts of the molecular template will allow for the development of future cascade active structures.

Acknowledgements

This work was supported by the MEXT Program for Promoting the Enhancement of Research Universities in NAIST and also partly supported by the JSPS KAKENHI Grant (JP26107006) in Scientific Research on Innovative Areas “Photosynergetics”. CJM thanks the JSPS for a KAKENHI Grant-in-Aid for Early-Career Scientists (19K15312) and RA thanks the NAIST foundation for financial support. Dr. Keiki Inoue is thanked for his kind assistance with compiling computational data. We also thank the NAIST technical staffs, Ms. Y. Nishikawa and Mr. F. Asanoma, for their kind support on MS- and NMR-measurements.

Notes and references

1 T. L. Lentz, *Cell fine structure*, Philadelphia, 1971.
2 B. Hille, *Ionic Channels of Excitable Membranes*, Oxford University Press Inc, 2001.
3 R. B. Emmons, *J. Appl. Phys.*, 1967, **38**, 3705.
4 S. Cova, M. Bertolaccini, C. Bussolati, *Phys. Status Solidi A*, 1973, **18**, 11–62.
5 V. O'Connor, D. Phillips, *Time-Correlated Single Photon Counting*, Academic, London, 1984.
6 H. Kume, K. Koyama, K. Nakatsugawa, S. Suzuki, D. Fatlowitz, *Appl. Opt.*, 1988, **27**, 1170–1178.
7 S. Cova, A. Lacaita, M. Ghioni, G. Ripamonti, T. A. Louis, *Rev. Sci. Instrum.*, 1989, **60**, 1104–1110.
8 H. Dautet, P. Deschamps, B. Dion, A. D. MacGregor, D. MacSween, R. J. McIntyre, C. Trottier, P. P. Webb, *Appl. Opt.*, 1993, **32**, 3894–3900.
9 S. Cova, M. Ghioni, A. Lacaita, C. Samori, F. Zappa, *Appl. Opt.*, 1996, **35**, 1956–1976.
10 M. Irie, *Chem. Rev.*, 2000, **100**, 1685-1716.
11 M. Irie, T. Fukaminato, K. Matsuda, S. Kobatake, *Chem. Rev.*, 2014, **114**, 12174-12277.
12 T. Nakashima, K. Atsumi, S. Kawai, T. Nakagawa, Y. Hasegawa, T. Kawai, *Eur. J. Org. Chem.*, 2007, **19**, 3212-3218.
13 Y. Kutsunugi, S. Kawai, T. Nakashima, T. Kawai, *New J. Chem.*, 2009, **33**, 1368-1373.
14 S. Fukumoto, T. Nakashima, T. Kawai, *Angew. Chem., Int. Ed.*, 2011, **50**, 1565-1568.
15 R Asato, C.J. Martin, T. Nakashima, J.P. Calupitan, G. Rapenne, T. Kawai, *J. Phys. Chem. Lett.*, 2021, **12**, 11391-11398.
16 T. Nakashima, K. Tsuchie, R. Kanazawa, R. Li, S. Iijima, O. Galangau, H. Nakagawa, K. Mutoh, Y. Kobayashi, J. Abe, T. Kawai, *J. Am. Chem. Soc.*, 2015, **137**, 7023-7026.
17 R. Li, T. Nakashima, R. Kanazawa, O. Galangau, T. Kawai, *Chem. Eur. J.*, 2016, **22**, 16250-16257.
18 O. Galangau, S. Delbaere, N. Ratel-Ramond, G. Rapenne, R. Li, J.P.D.C. Calupitan, T. Nakashima, T. Kawai, *J. Org. Chem.*, 2016, **81**, 11282-11290.
19 R. Li, T. Nakashima, T. Kawai, *Chem. Commun.*, 2017, **53**, 4339-4341.
20 C. Martin, M. Minamide, J. Calupitan, R. Asato, J. Kuno, T. Nakashima, G. Rapenne and T. Kawai, *J. Org. Chem.*, 2018, **83**, 13700-13706.
21 C. J. Martin, J. P. Calupitan, M. Minamide, R. Asato, Y. Goto, G. Rapenne, T. Nakashima and T. Kawai, *J. Photochem. Photobiol. A: Chem.*, 2020, **397**, 112594.
22 R. Mizutsu, R. Asato, C. J. Martin, M. Yamada, Y. Nishikawa, S. Katao, M. Yamada, T. Nakashima, T. Kawai, *J. Am. Chem. Soc.*, 2019, **141**, 20043-20047.
23 A. Griesbeck, N. Hoffmann and K. Warzecha, *Acc. Chem. Res.*, 2007, **40**, 128–140.
24 W. Waddell, C. Lee, *J. Am. Chem. Soc.*, 1982, **104**, 5804–5805.
25 C. Marquez, H. Wang, F. Fabbretti, J. Metzger, *J. Am. Chem. Soc.*, 2008, **130**, 17208–17209,

26 T. Yorozu, K. Yoshida, K. Hayashi, M. Irie, *J. Phys, Chem*., 1981, **85**, 459-462.
27 T. Arai, T. Karatsu, H. Sakuragi, K. Tokumaru. *Tetrahedron Lett*., 1983, **24**, 2873-2876.
28 G. Kuzmanich, M. Gard, M. Garcia-Garibay, *J. Am. Chem. Soc.*, 2009, **131**, 11606–11614.
29 T. Koshido, T. Kawai, K. Yoshino, *J. Phys Chem.*, 1995, **99**, 6110-6114.
30 A. Peters, N. Branda, *J. Am. Chem. Soc.*, 2003, **125**, 3404–3405.
31 W. Browne, J. de Jong, T. Kudernac, M. Walko, L. Lucas, K. Uchida, J. van Esch, B. Feringa, *Chem. Eur. J.*, 2005, **11**, 6430–6441.
32 B. Corodetsky, N. Branda, *Adv. Funct. Mater.*, 2007, **17**, 786–796.
33 J. Massaad, J. C. Micheau, C. Coudret, C. L. Serpentini, G. Guirado, *Chem. Eur. J.,* 2013, **19**, 12435-12445.
34 M. Kishida, T. Kusamoto, H. Nishihara, *J. Am. Chem. Soc.*, 2014, **136***,* 4809–4812.
35 S. Lee, Y. You, K. Ohkubo, S. Fukuzumi, *Chem. Sci.,* 2014, **5**, 1463-1474.
36 T. Nakashima, Y. Kajiki, S. Fukumoto, M. Taguchi, S. Nagao, S. Hirota, T. Kawai, *J. Am. Chem. Soc.*, 2012, **134**, 19877–19883.
37 J. Calupitan, T. Nakashima, Y. Hashimoto, T. Kawai, *Chem. Eur. J.*, 2016, **22**, 10002-10008.
38 R. Asato, C. Martin, J. Calupitan, R. Mizutsu, T. Nakashima, G. Okada, N. Kawaguchi, T. Yanagida, T. Kawai, *Chem. Sci.*, 2020, **11**, 2504-2510.
39 W. Li, C. Jiao, X. Li., Y. Xie, K. Nakatani, H.Tan, W. Zhu, *Angew. Chem., Int. Ed.*, 2014, **53**, 4603-4607.
40 M. Li, W. Zhu, *Acc. Chem. Res.*, 2022, **55**, 3136-3149.
41 M. J. Frisch et al. (see Supporting Information for full author list) *Gaussian 09 Revision A.02*, Gaussian Inc. Wallingford CT, 2009.
42 Y. Moriyama, K. Matsuda, N. Tanifuji, S. Irie, M. Irie, *Org. Lett.*, 2005, **7**, 3315–3318.

Supplementary Information

FIGURES

Experimental details

^{1}H and ^{13}C NMR (400 and 600 MHz) spectra were recorded on, *JEOL* JNM-ECP400 and *JEOL* JNMECA600 spectrometers, respectively. High-resolution mass spectrometry were performed on matrix assisted laser desorption/ionization (MALDI) time of Flight (TOF) – MS spectra (*Bruker* Autoflex II or *JEOL* spiralTOF JMS-S3000). Recycling preparative GPC were performed on *Japan Analytical Industry* LC-9110NEXT. UV/Vis spectra, quantum yields of photochromic reactions ($\phi_{o\text{-}c}$ and $\phi_{c\text{-}o}$) and photo-induced fading reactions were measured using a *JASCO* V-660, V-760 spectrophotometer and a *Shimadzu* QYM-01 set-up. All illuminations were performed in the dark at room temperature in high grade HPLC solvents that were stored under argon, used without further purification and pre-bubbled with nitrogen gas for 30 minutes before solid dissolution where necessary.

UV-induced cycloreversion experiments were performed on the photo stationary state (PSS) generated in toluene through irradiation with a LED-UV light at 365 nm followed by dilution with chloroform, monitoring the evolution of absorbance at λ_{max} with constant stirring to avoid the effect of diffusion on the electron transfer. Oxidative cycloreversion experiments were performed by mixing the requisite amounts of the oxidizing agent tris(4-bromophenyl)ammonium hexachloroantimonate (TBPA) with a photogenerated PSS in acetonitrile and monitoring the evolution of absorbance at λ_{max}, with constant stirring to avoid the effect of diffusion on the electron transfer. Cyclic voltammetry measurements were performed with an ALS electrochemical analyser Model 630DA at room temperature working under an argon atmosphere, equipped with a 3 mm diameter glassy carbon working electrode, a Pt wire counter electrode and Ag/Ag^{+} reference electrode at a scan rate of 100 mV s^{-1} at 20°C. Samples were run in HPLC grade acetonitrile deoxygenated by argon bubbling for at least 20 min, containing 0.1 M $TBAPF_6$ as supporting electrolyte at initial concentrations of 1 mmol in a standard one-component cell; the obtained values were converted into those of Fc/Fc^{+} based on the measured redox potential of ferrocene. $TBAPF_6$ used as electrolyte was recrystallized from ethanol and dried under reduced pressure for 12 h at 100°C. Ferrocene was sublimated under reduced pressure at 80°C. PSS Solutions for voltammetry were generated via illumination of the open form at 365 nm in 20 mL of high-grade toluene. The mass of solid present was such that upon removal of toluene and redissolution in 5 mL of electrolyte a 1 mmol PSS (open + closed) was formed.

Calculations were performed with the Gaussian09 package.[1] We worked at the B3LYP 6-31+G(d,p) level of theory in vacuo. The open form as drawn with the reactive carbons relatively close to each other were used as input structures. Frequency calculation showed no negative frequencies confirming that resulting structures were in the absolute minima of the potential map. Kinetic curve fittings were carried out, with calculated values for [**C**], [$\mathbf{C}^{\cdot+}$], [**O**] and [$\mathbf{O}^{\cdot+}$] generated using an initial experimental concentration of 5.59×10^{-6} M along with the

kinetic parameters and equations show in Figure 11. These were then used to generate a calculated decay in absorption over time (A_{calc}) using the experimentally estimated absorption coefficient of 9090 $M^{-1}cm^{-1}$ at the absorption maximum, this was then compared to the measured decay (A_{exp}). The residual square difference $R_s = (A_{exp}-A_{Calc})^2$ between the calculated and experimental absorption was calculated for each data point and then all values of R_s summed to give a residual sum of squares (R). R was then minimised computationally, with constant values of k_1, k_2, k_5 and k_6 determined as described in the main text, in a three variable ([C]: [$C^{+\cdot}$], k_3 and k_4) optimisation using the SOLVER software, adjusting the kinetic parameters to give a minimum value for R.

General Synthesis

All reagents and solvents were purchased at the highest commercial quality available and used without further purification, unless otherwise stated. Compounds **S4, S11** and **1o**-**4o** were prepared according to the routes depicted in Schemes S1 to S6. Compounds **5o,**[2] **6o,** [2] **S12,**[3] **S13,**[4] **S15**[2] and **S16**[2] were synthesized as previously reported and compounds **S1** and **S5** were commercially available. The final structures of **1o**-**4o** have all been successfully characterised using NMR and HR-MS which are shown in Figures S1-S12.

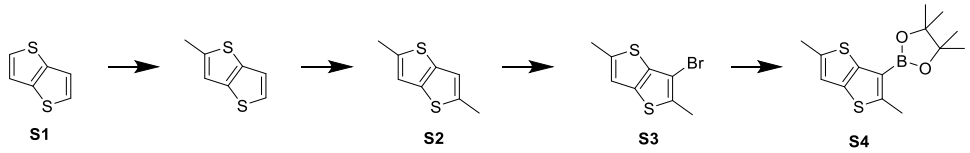

Scheme S1. *Synthesis of key intermediate* ***S4****.*

S2: 2,5-dimethylthieno[3,2-b]thiophene: Thieno[3,2-b]thiophene **S1** (3.50 g, 24.96 mmol) was dissolved in tetrahydrofuran (200 mL) and cooled to -40°C. To this solution n-butyllithium (2.5 M, 12.98 mL, 32.45 mmol) was added dropwise and the solution was stirred for 45 min at -40°C. To this, methyl iodide (2.02 mL, 32.45 mmol) was added dropwise over 20 min and the solution warmed to room temperature. Water was added and the solution extracted with ethyl acetate, dried over magnesium sulfate and solvent removed under vacuum. The solid was dissolved in hexane and passed through a short silica column (1st spot Rf = 0.8) to give intermediate 2-

methylthieno[3,2-b]thiophene that was then dissolved in tetrahydrofuran (200 mL) and cooled to -40°C. To this solution n-butyllithium (2.5 M, 12.98 mL, 32.45 mmol) was added dropwise and the solution was stirred for 45 min at -40°C. To this, methyl iodide (2.02 mL, 32.45 mmol) was added dropwise over 20 min and the solution warmed to room temperature. Water was added and the solution extracted with ethyl acetate, dried over magnesium sulfate and solvent removed under vacuum. The solid was dissolved in hexane and passed through a short silica column (1st spot Rf = 0.8) to give pure white crystals. **Yield:** 3.07 g, 18.24 mmol, 73% over two steps. **^{1}H-NMR** (400 MHz, $CDCl_3$, 25°C) δ: 6.87 (m, 2H), 2.59 (d, 6H, J = 1.3).

S3: 3-bromo-2,5-dimethylthieno[3,2-b]thiophene: To a solution of **S2** (1.5 g, 8.91 mmol) in a 1:1 mix of glacial acetic acid: chloroform (160 mL) was added n-bromosuccinimide (1.75 g, 9.81 mmol) and the solution stirred for 16 hours. Then 2 M aqueous potassium hydroxide was added until the solution reached a pH of 5 and then a saturated aqueous solution of sodium thiosulfate was added. The solution was extracted into dichloromethane, washed with water, dried over magnesium sulfate, filtered and solvent removed. Silica gel column chromatography (1st spot, Rf = 0.9 in hexane) gave the product as a white solid. **Yield:** 1.74 g, 7.08 mmol, 79%. **^{1}H-NMR** (400 MHz, $CDCl_3$, 25°C) δ: 6.92 (q, 1H, J = 1.2 Hz), 2.60 (d, 3H, J = 1.2 Hz), 2.51 (s, 3H).

S4: 2-{2,5-dimethylthieno[3,2-b]thiophen-3-yl}-4,4,5,5-tetramethyl-1,3,2-dioxaborolane: To a solution of **S3** (900 mg, 3.64 mmol) in tetrahydrofuran (30 mL) under inert atmosphere, n-butyl lithium (1.6 M, 2.50 mL, 4.01 mmol) was added dropwise at –78°C and the mixture stirred for 2 hours at that temperature. 2-Isopropoxy-4,4,5,5-tetramethyl-1,3,2-dioxaborolane (0.89 mL, 4.37 mmol) was then added dropwise and the system was stirred for another 2 hours at –78°C. The reaction mixture was allowed to warm to room temperature over 3 hours and then methanol (40 mL) added and the solution extracted with ethyl acetate. The combined organic fraction was washed with water, dried over anhydrous magnesium sulfate, and concentrated to a yellow oil. Silica gel column chromatography (3rd spot Rf = 0.6 in 2:1 hexane: dichloromethane) gave the product as a yellow solid. **Yield:** 835 mg, 2.84 mmol, 78%. **^{1}H-NMR** (400 MHz, $CDCl_3$, 25°C) δ: 6.82 (q, 1H, J = 1.3 Hz), 2.74 (s, 3H), 2.54 (d, 3H, J = 1.3 Hz), 1.35 (s, 12H).

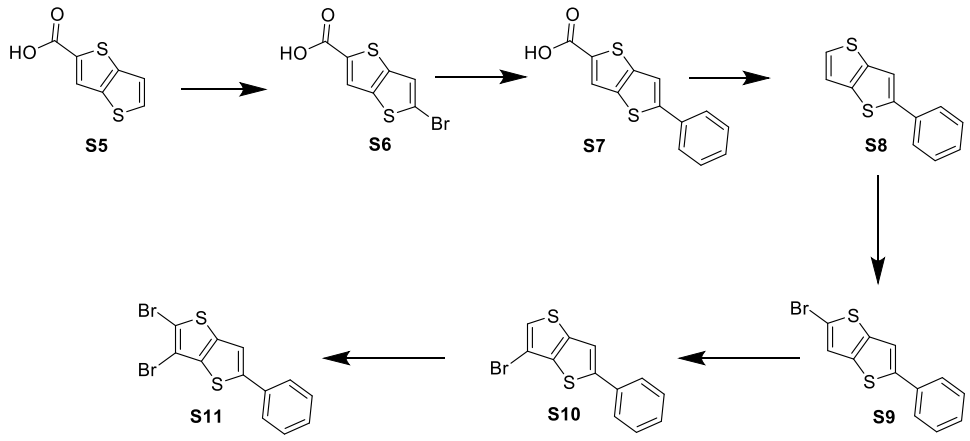

Scheme S2. *Synthesis of key intermediate* ***S9****.*

S6: 5-bromothieno[3,2-b]thiophene-2-carboxylic acid: Thieno[3,2-b]thiophene-2-carboxylic acid **S5** (5.0 g, 27.13 mmol) was dissolved in dimethylformamide (50 mL) at 0°C. n-Bromosuccinimide (4.927 g, 27.66 mmol) was added and the reaction mixture stirred for 3 hours. Water (50 mL) was added and the mixture stirred for 30 min as a white precipitate formed. The precipitate was filtered off and recrystallized from water. This was dried in a desiccator in the presence of phosphorous pentoxide to give a white solid that was used crude in the next step. **Yield:** 4.31 g.

S7: 5-phenylthieno[3,2-b]thiophene-2-carboxylic acid: Under an inert atmosphere, **S5** (4.285 g, 16.29 mmol) and phenyl boronic acid (2.085 g, 17.1 mmol) were dissolved in tetrahydrofuran (190 mL). Tetrakis(triphenyphosphine) palladium 0 (376 mg, 0.326 mmol), potassium carbonate (6.752 g, 48.86 mmol) and water (60 mL) were added and the solution refluxed for 24 hours. Upon cooling to room temperature more water (200 mL) was added. All solvents except water were removed under vacuum and the solution cooled at 0°C giving a white precipitate which was dissolved in hot water, acidified by addition of 1M aqueous hydrochloric acid and cooled again to give a solid that was collected by filtration. This was dried in a desiccator in the presence of phosphorous pentoxide to give the product as a white solid. **Yield:** 3.61 g, 13.87 mmol, 85%. **^{1}H-NMR** (400 MHz, d-DMSO, 25°C) δ: 13.30 (br-s, 1H), 8.12 (s, 1H), 7.95 (s, 1H), 7.73 (m, 2H), 7.48 (m, 2H), 7.39 (m, 1H).

S8: 2-phenylthieno[3,2-b]thiophene: Under an inert atmosphere, **S7** (1.90 g, 7.30 mmol) was dissolved in quinoline (25 mL), copper powder (232 mg, 3.65 mmol) was added and the resulting mixture was heated to 225°C for 3 hours. Quinoline was distilled off under reduced pressure and

the residue dissolved in ethyl acetate and filtered through celite. The resulting solution was washed three times with dilute aqueous hydrochloric acid (1 M), and then washed three times with water. After drying over anhydrous magnesium sulfate, the solvent was evaporated to give a yellow solid. Silica gel column chromatography (1st spot Rf = 0.3 in hexane) followed by recrystallization from ethanol gave the product as a yellow solid. **Yield:** 1.154 g, 5.335 mmol, 73%. **^{1}H-NMR** (400 MHz, $CDCl_3$, 25°C) δ: 7.68 (m, 2H), 7.53 (d, 1H, J = 0.6 H), 7.48-7.38 (m, 3H), 7.35 (tt, 1H, J = 9.8 and 1.7 Hz), 7.29 (dd, 1H, J = 7.0 and 0.6 Hz).

S9: 2-bromo-5-phenylthieno[3,2-b]thiophene: S8 (1.154 g, 5.335 mmol) was dissolved in dimethylformamide (11 mL) at 0°C. n-Bromosuccinimide (969 mg, 5.441 mmol) was added and the reaction mixture stirred for 3 hours. Water (20 mL) was added and the mixture extracted with dichloromethane, washed three times with water, dried over anhydrous magnesium sulfate and concentrated to a yellow oil. This was dissolved in 1:1 hexane: dichloromethane and passed through a short silica column (1st spot Rf = 0.8) to give the product as a yellow solid. **Yield:** 1.24 g, 4.20 mmol, 79%. **^{1}H-NMR** (400 MHz, $CDCl_3$, 25°C) δ: 7.64 (m, 2H), 7.44 (m, 3H), 7.35 (tt, 1H, J = 9.7 and 1.8 Hz), 7.29 (d, 1H, J = 4.0 Hz).

S10: 6-bromo-2-phenylthieno[3,2-b]thiophene: Freshly prepared lithium diisopropylamide (2.07 mmol) in tetrahydrofuran (9 mL) at 0°C was added dropwise over 30 minutes to a solution of **S9** (1.24 g, 4.20 mmol) in tetrahydrofuran (16 mL) cooled to –78°C and then stirred for 90 min at –78°C. Methanol (7 mL) was added and the solution stirred 30 min at –78°C followed by 16 hours at room temperature. Water was added and the solution extracted with chloroform, washed with brine, then with water, dried over anhydrous magnesium sulfate and concentrated to an orange solid. This was dissolved in chloroform and passed through a short silica column (1st spot Rf = 0.8) to give the product as a yellow solid. **Yield:** 1.08 g, 3.66 mmol, 87%. **^{1}H-NMR** (400 MHz, $CDCl_3$, 25°C) δ: 7.69-7.62 (m, 2H), 7.51 (s, 1H), 7.49-7.34 (m, 4H).

S11: 2,3-dibromo-5-phenylthieno[3,2-b]thiophene: S10 (1.08 g, 3.66 mmol) and n-bromosuccinimide (977 mg, 5.488 mmol) were dissolved in chloroform (40 mL) and refluxed for 16 hours. An aqueous sodium thiosulfate solution was added and the mixture extracted with chloroform. The organic layer was washed with water, dried over anhydrous magnesium sulfate and concentrated to an orange solid. This was dissolved in chloroform and passed through a short silica column (1st spot Rf = 0.8) to give the product as an off white solid. **Yield:** 1.151 g, 3.077 mmol, 84%. **^{1}H-NMR** (400 MHz, $CDCl_3$, 25°C) δ: 7.67-7.62 (m, 2H), 7.49-7.33 (m, 4H).

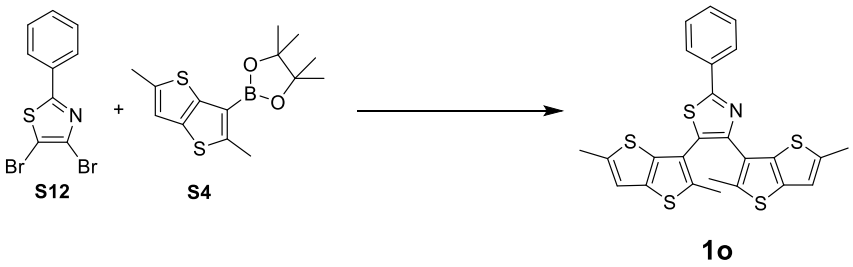

Scheme S3. *Synthesis of compound* ***1o****.*

1o: To a solution of **S12**[3] (500 mg, 1.567 mmol), **S4** (968 mg, 3.291 mmol) and triphenylphosphine (206 mg, 0.784 mmol), in 2M aqueous tripotassium phosphate (75 mL) and 1,4-dioxane (75 mL) was added tetrakis(triphenyphosphine) palladium 0 (181 mg, 0.157 mmol) and the solution refluxed at 100°C for 3 days. The solution was quenched with 2M aqueous hydrochloric acid and extracted to ethyl acetate, washed three times with water, dried over anhydrous magnesium sulfate and concentrated to a yellow solid. Silica gel column chromatography (1st spot Rf = 0.7 in 9:1 hexane: ethyl acetate) gave the product as a white solid that turned blue under UV light. **Yield:** 480 mg, 0.972 mmol, 62%. **^{1}H-NMR** (600 MHz, $CDCl_3$, 25°C) δ: 8.06 (m, 2H), 7.45 (m, 3H), 6.84 (m, 1H), 6.82 (m, 1H), 2.53 (m, 6H), 2.05 (s, 3H), 2.02 (s, 3H). **^{13}C-NMR** (151 MHz, $CDCl_3$, 25°C) δ: 166.8, 147.7, 141.1, 138.7, 138.4, 138.3, 138.1, 134.8, 134.6, 133.6, 130.3, 129.0, 127.4, 127.0, 126.6, 125.3, 121.0, 117.6, 117.1, 16.5, 16.4, 15.4, 15.2. **HRMS:** m/z 439.0112 ($[M]^+$) (calc. 439.0116).

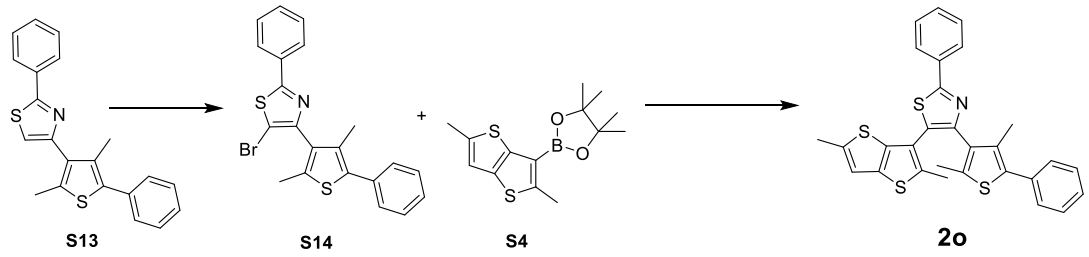

Scheme S4. *Synthesis of compound* ***2o****.*

S14: S13[4] (780 mg, 2.25 mmol) was dissolved in a mixture of chloroform (70 ml) and glacial acetic acid (7 mL). To this n-bromosuccinimide (479 mg, 2.69 mmol) was added and the solution heated under reflux at 60°C for 16 hours. The solution was quenched with water and extracted into chloroform, washed with brine and then water, dried over dried over anhydrous magnesium sulfate and concentrated to a yellow solid. This was dissolved in dichloromethane and passed through a short silica column (1st spot Rf = 0.8) to give the product as a yellow solid. **Yield:** 347 mg, 0.814 mmol, 36%. **^{1}H-NMR** (400 MHz, $CDCl_3$, 25°C) δ: 7.97 (m, 2H), 7.55-7.40 (m, 7H), 7.35 (tt, 1H, J = 9.7 and 1.2 Hz), 2.44 (s, 3H), 2.19 (s, 3H).

2o: S14 (347 mg, 0.814 mmol), **S4** (311 mg, 1.058 mmol) and tripotassium phosphate (259 mg, 1.221 mmol) were cycled between argon and vacuum 3 times. Then tetrakis(triphenyphosphine) palladium 0 (28 mg, 0.024 mmol) was added and the system cycled between argon and vacuum 3 more times. 1,2-dimethoxyethane (40 mL) and water (20 mL) were then added and the solution heated to 70°C for 24 hours. The mixture was cooled to room temperature and water added followed by extraction into ethyl acetate, washed with brine then with water, dried over anhydrous magnesium sulfate and concentrated to give a yellow solid. Silica gel column chromatography (2nd spot Rf = 0.6 in 20:1 hexane: ethyl acetate) gave a solid that was further purified by GPC in chloroform to give a white solid that turned blue under UV light. **Yield:** 290 mg, 0.564 mmol, 69%. **^{1}H-NMR** (600 MHz, $CDCl_3$, 25°C) δ: 8.04 (m, 2H), 7.49-7.35 (m, 7H), 7.28 (dt, 1H, J = 6.9 and 1.8 Hz), 6.84 (q, 1H, 1.2 Hz), 2.53 (d, 3H, J = 1.2 Hz), 2.14 (s+s, 6H), 2.04 (s, 3H). **^{13}C-NMR** (151 MHz, $CDCl_3$, 25°C) δ: 166.4, 149.4, 141.1, 138.7, 138.0, 137.3, 135.2, 135.0, 134.7, 134.0, 133.7, 133.0, 130.3, 129.3, 129.0, 128.5, 128.2, 127.0, 126.6, 121.0, 117.5, 16.4, 15.0, 14.9, 14.3. **HRMS:** m/z 513.0707 ($[M]^+$) (calc. 513.0708).

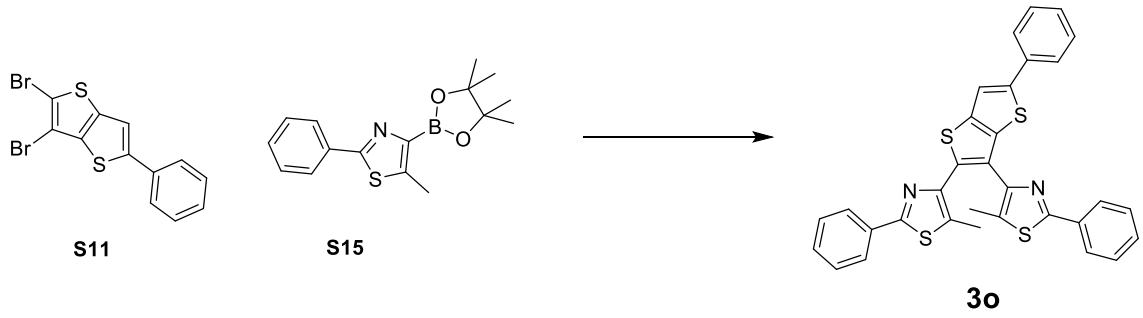

Scheme S5. *Synthesis of compound **3o**.*

3o: S11 (296 mg, 0.79 mmol), **S15**[2] (500 mg, 1.66 mmol), triphenylphosphine (104 mg, 0.395 mmol) and tripotassium phosphate (587 mg, 2.765 mmol) were dissolved in a mixture of 1,4-dioxane (70 mL) and water (30 mL). Then tetrakis(triphenyphosphine) palladium 0 (91 mg, 0.079 mmol) was added and the solution refluxed at 110°C for 72 hours. The mixture was cooled to room temperature and quenched with 1M aqueous hydrochloric acid followed by extraction into ethyl acetate, washed with brine then with water, dried over anhydrous magnesium sulfate and concentrated to give an orange solid. Silica gel column chromatography (1st spot Rf = 0.8 in 20:1 hexane: ethyl acetate) gave a solid that was further purified by GPC in chloroform to give a white solid that turned blue under UV light. **Yield:** 121 mg, 0.215 mmol, 27%. **^{1}H-NMR** (600 MHz, $CDCl_3$, 25°C) δ: 8.02 (m, 2H), 7.94 (m, 2H), 7.68 (m, 2H), 7.53 (s, 1H), 7.48-7.38 (m, 8H), 7.30 (m, 1H), 2.05 (s, 3H), 2.01 (s, 3H). **^{13}C-NMR** (151 MHz, $CDCl_3$, 25°C) δ: 164.9, 164.7, 147.1, 146.7, 146.5, 140.2, 138.9, 135.0, 134.7, 133.7, 133.5, 131.2, 131.1, 130.1, 130.0, 129.1, 129.0, 129.0, 127.9, 126.6, 126.5, 126.4, 126.1, 115.5, 12.5, 12.3. **HRMS:** m/z 562.0662 ($[M]^+$) (calc. 562.0660)

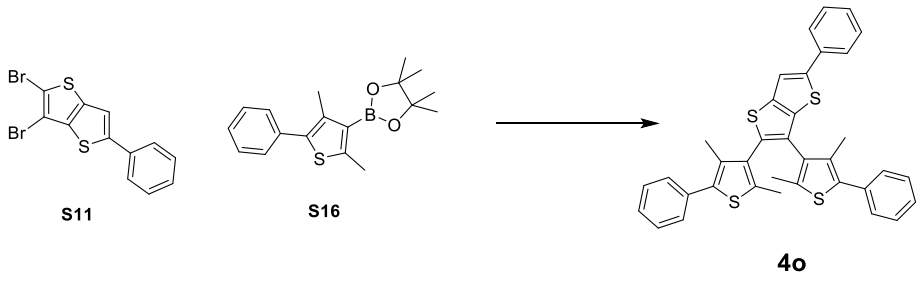

Scheme S6. *Synthesis of compound* ***4o****.*

4o: S11 (284 mg, 0.76 mmol), **S16**[2] (500 mg, 1.59 mmol), triphenylphosphine (104 mg, 0.397 mmol) and tripotassium phosphate 563 mg, 2.653 mmol) were dissolved in a mixture of 1,4-dioxane (70 mL) and water (30 mL). Then tetrakis(triphenyphosphine) palladium 0 (91 mg, 0.079 mmol) was added and the solution refluxed at 110°C for 72 hours. The mixture was

cooled to room temperature and quenched with 1M aqueous hydrochloric acid followed by extraction into ethyl acetate, washed with brine then with water, dried over anhydrous magnesium sulfate and concentrated to give a yellow solid. Silica gel column chromatography (1^{st} spot Rf = 0.8 in 4:1 hexane: ethyl acetate) gave a solid that was further purified by GPC in chloroform to give a white solid that turned blue under UV light. **Yield:** 126 mg, 0.214 mmol, 28%. **^{1}H-NMR** (600 MHz, $CDCl_3$, 25°C) δ: 7.65 (m, 2H), 7.54 (s, 1H), 7.47-7.36 (m, 10H), 7.34-7.27 (m, 3H), 2.32-2.00 (m, 12 H, CH_3 signals broadened by conformational isomers). **^{13}C-NMR** (151 MHz, $CDCl_3$, 25°C) δ: Signals split by isomerization. **HRMS:** m/z 588.1069 ($[M]^+$) (calc. 588.1068).

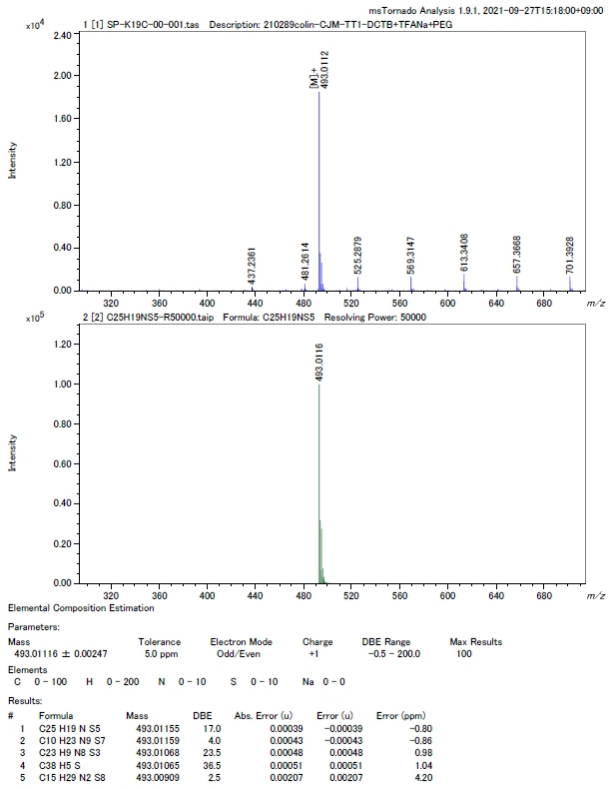

Elemental Composition Estimation

Parameters:

Mass	Tolerance	Electron Mode	Charge	DBE Range	Max Results
493.01116 ± 0.00247	5.0 ppm	Odd/Even	+1	−0.5 – 200.0	100

Elements

C 0 – 100 H 0 – 200 N 0 – 10 S 0 – 10 Na 0 – 0

Results:

#	Formula	Mass	DBE	Abs. Error (u)	Error (u)	Error (ppm)
1	C25 H19 N S5	493.01155	17.0	0.00039	−0.00039	−0.80
2	C10 H23 N9 S7	493.01159	4.0	0.00043	−0.00043	−0.86
3	C23 H9 N8 S3	493.01068	23.5	0.00048	0.00048	0.98
4	C38 H5 S	493.01065	36.5	0.00051	0.00051	1.04
5	C15 H29 N2 S8	493.00909	2.5	0.00207	0.00207	4.20

Figure S1. HR-MS data measurement (top) and calculation result (bottom) of **1o**. MALDI-Spiral-TOF system with polyethylene glycol as internal standard.

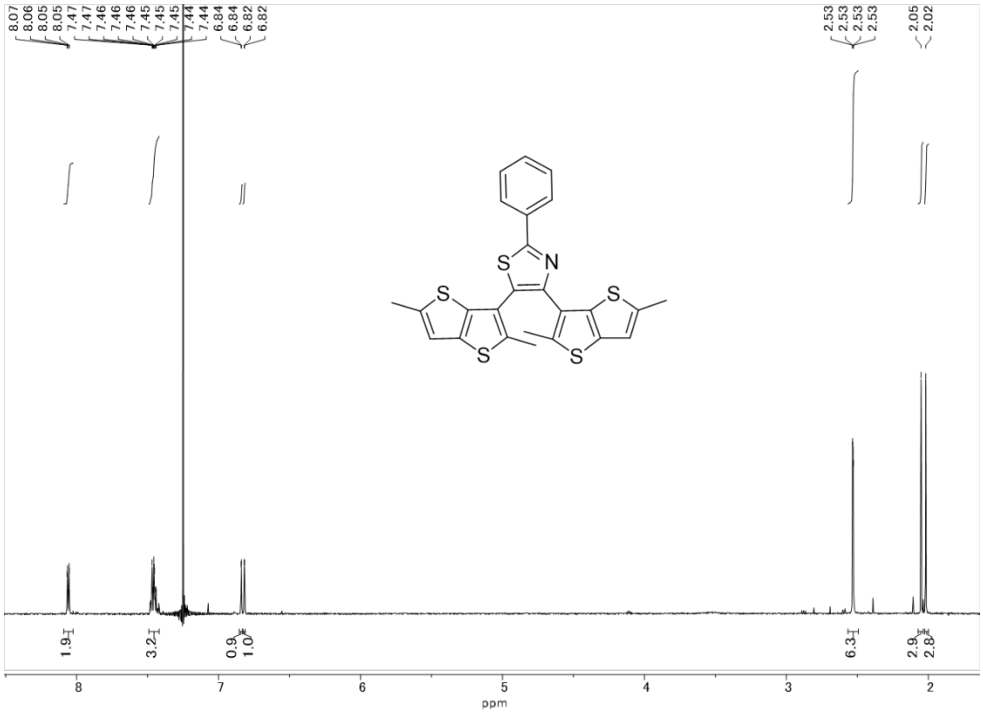

*Figure S2. ^{1}H NMR spectrum of **1o** (600 MHz, $CDCl_3$, TMS, 25°C).*

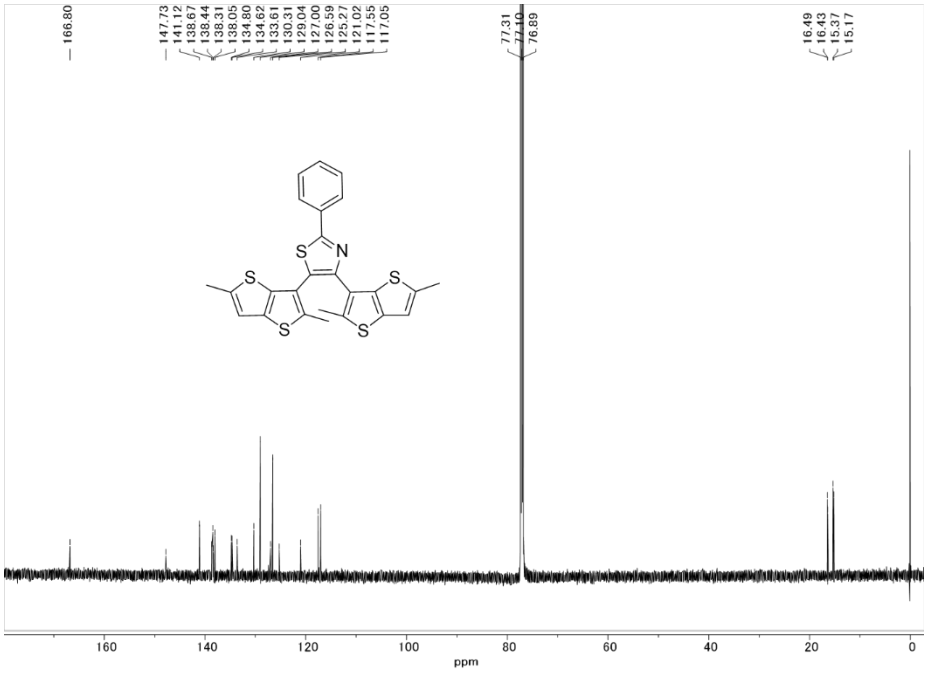

*Figure S3. ^{13}C NMR spectrum of **1o** (151 MHz, $CDCl_3$, TMS, 25°C).*

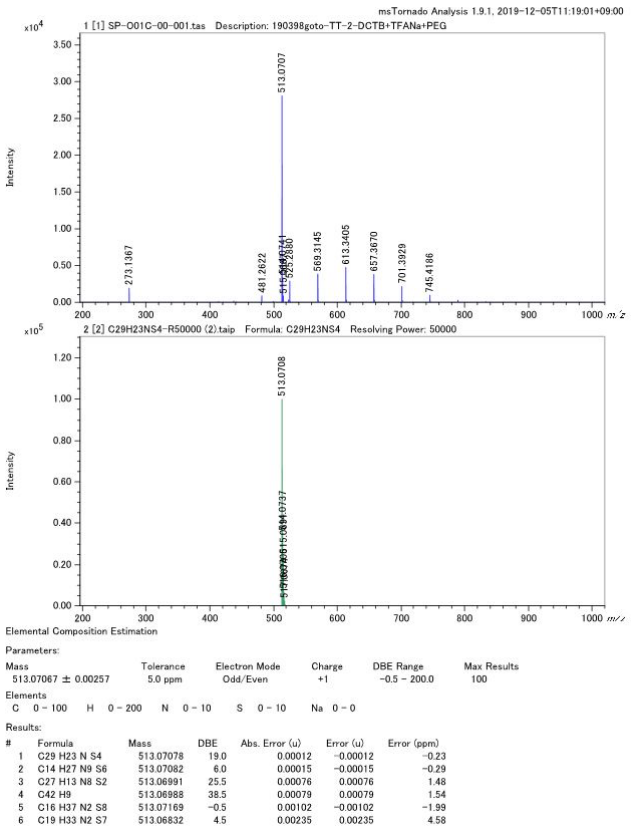

*Figure S4. HR-MS data measurement (top) and calculation result (bottom) of **2o**. MALDI-Spiral-TOF system with polyethylene glycol as internal standard.*

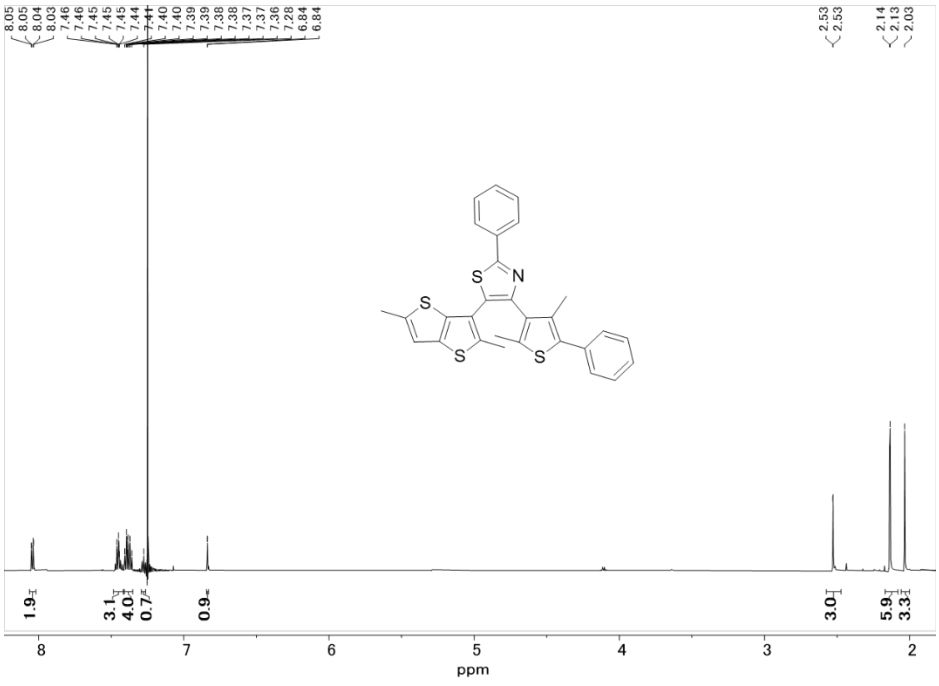

*Figure S5. ^{1}H NMR spectrum of **2o** (600 MHz, $CDCl_3$, TMS, 25°C).*

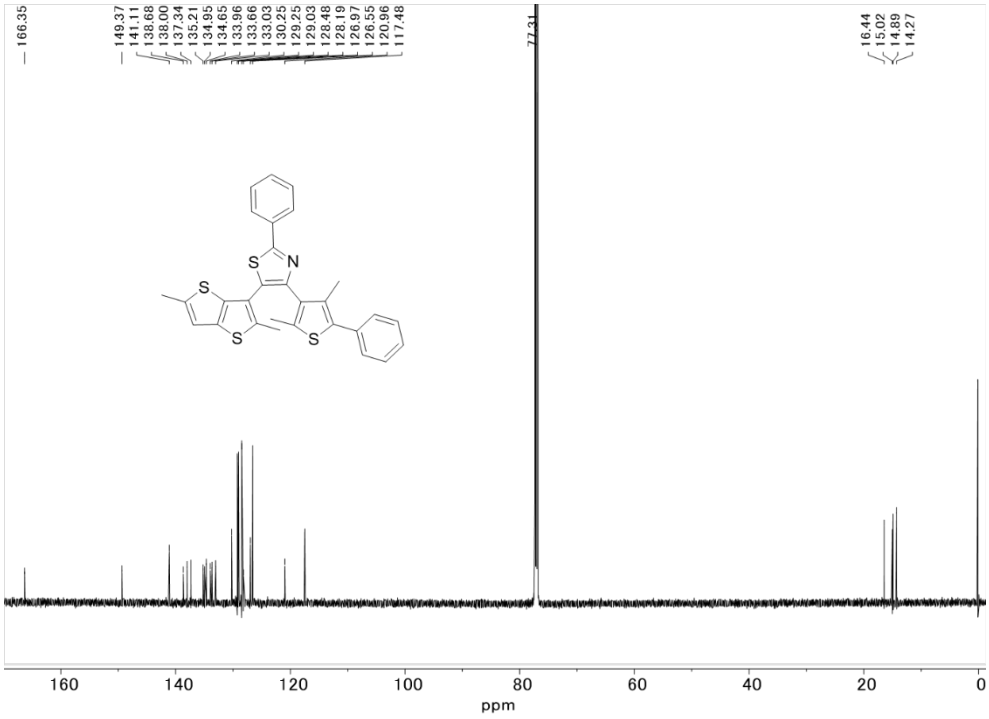

*Figure S6. ^{13}C NMR spectrum of **2o** (151 MHz, $CDCl_3$, TMS, 25°C).*

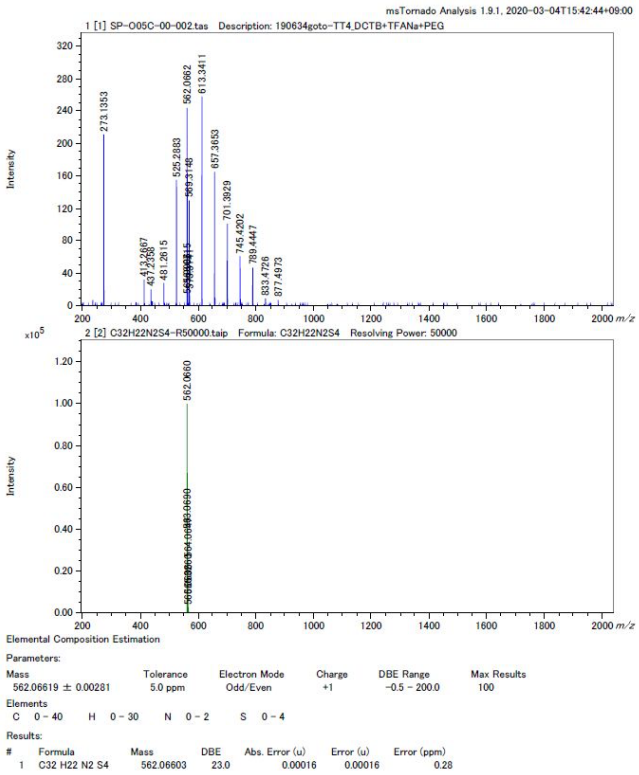

*Figure S7. HR-MS data measurement (top) and calculation result (bottom) of **3o**. MALDI-Spiral-TOF system with polyethylene glycol as internal standard.*

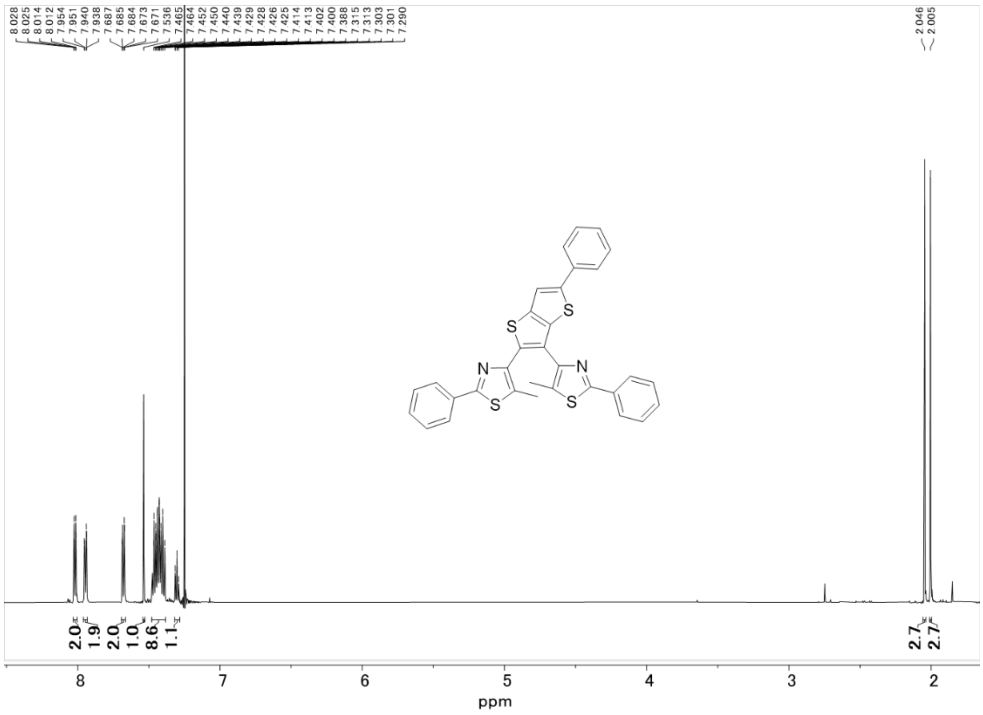

*Figure S8. ^{1}H NMR spectrum of **3o** (600 MHz, $CDCl_3$, TMS, 25°C).*

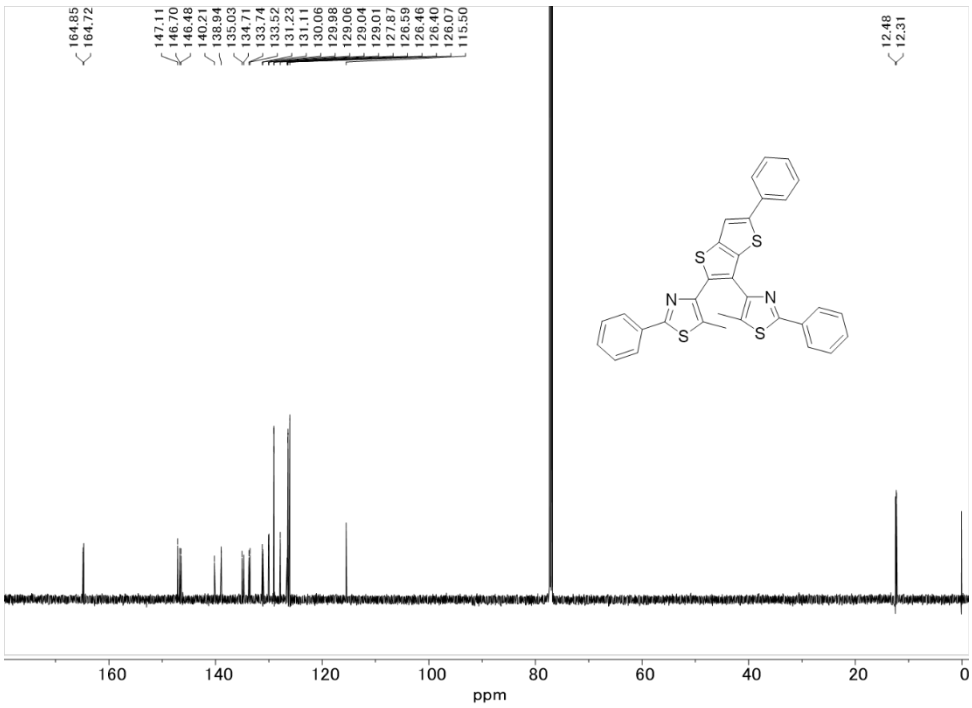

*Figure S9. ^{13}C NMR spectrum of **3o** (151 MHz, $CDCl_3$, TMS, 25°C).*

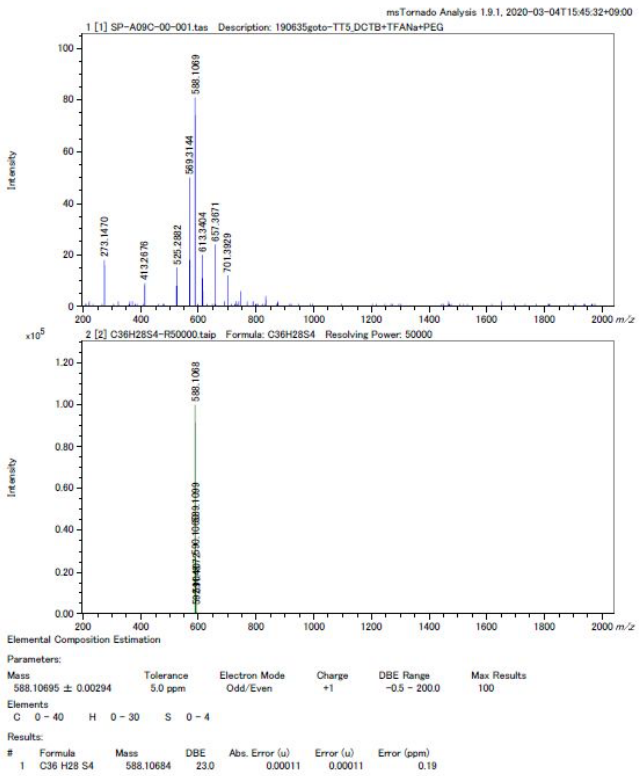

*Figure S10. HR-MS data measurement (top) and calculation result (bottom) of **4o**. MALDI-Spiral-TOF system with polyethylene glycol as internal standard.*

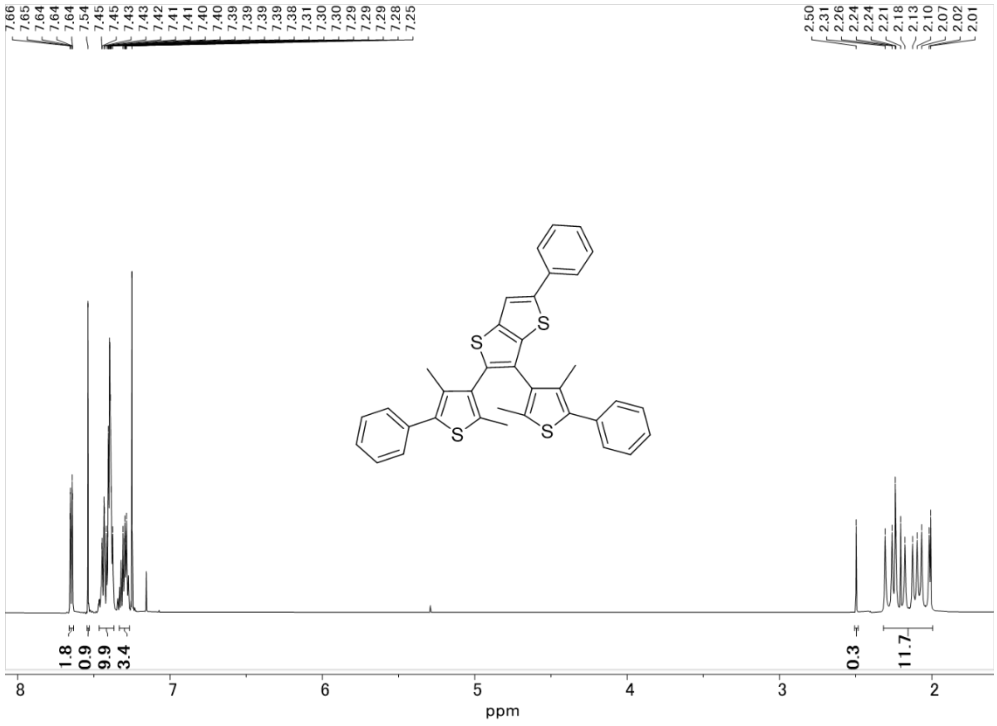

*Figure S11. ^{1}H NMR spectrum of **4o** (600 MHz, $CDCl_3$, TMS, 25°C).*

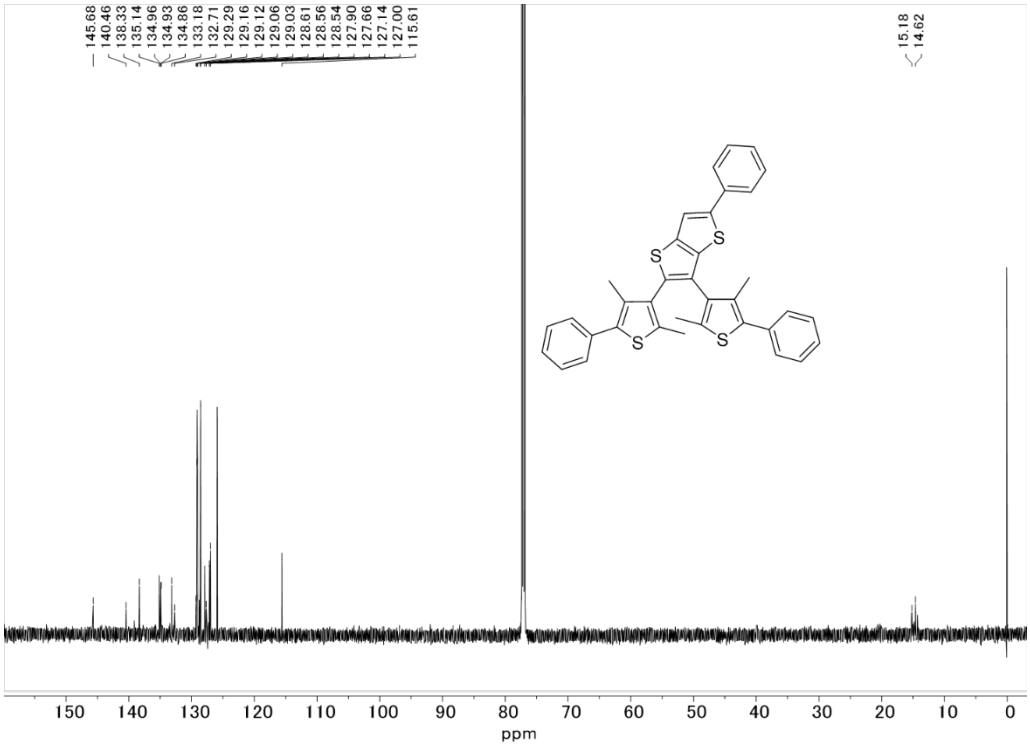

*Figure S12 ^{13}C NMR spectrum of **4o** (151 MHz, $CDCl_3$, TMS, 25°C).*

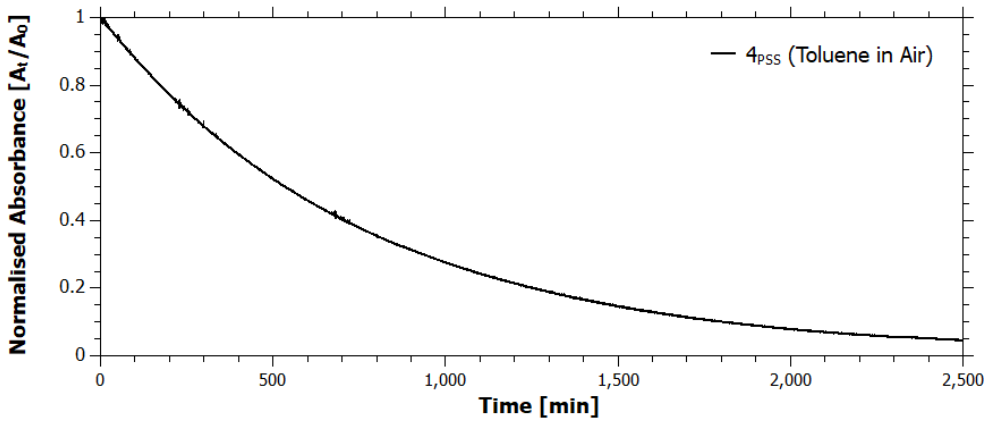

*Figure S13. Thermal decay in absorbance at λ_{max} of a PSS solution of **4** in toluene under air.*

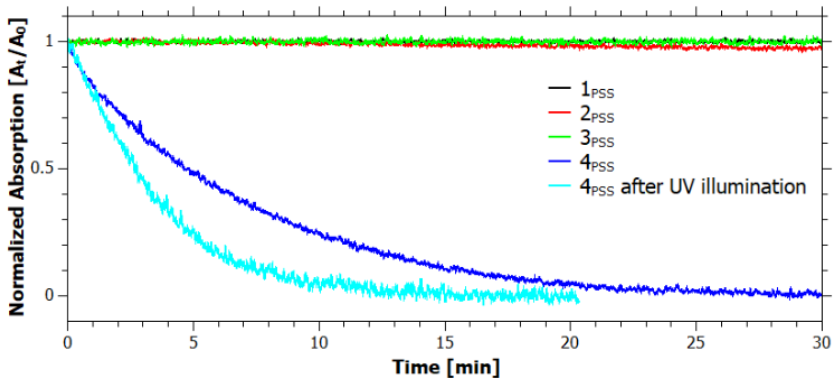

*Figure S14. Thermal decay in absorbance at λ_{max} of PSS solutions of **1**-**4** in 9:1 chloroform: toluene.*

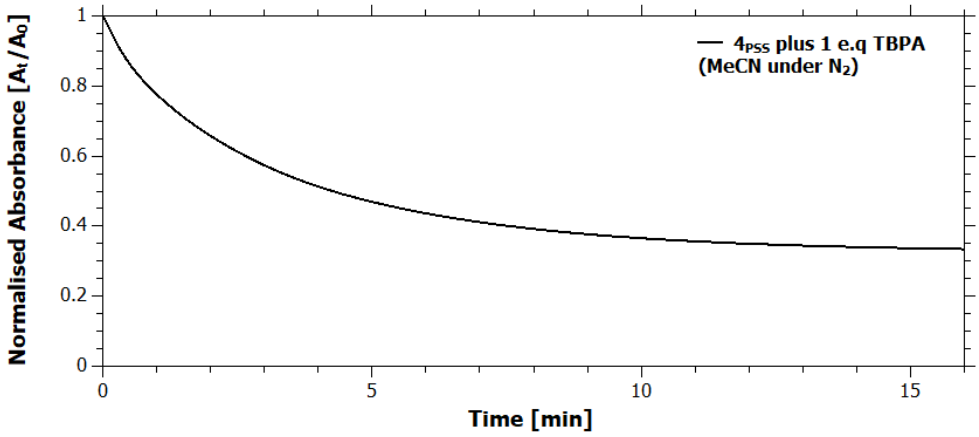

*Figure S15. Decay in absorbance at λ_{max} of a PSS solution of **4** in acetonitrile upon addition of 1 eq. of TBPA, showing the decay of a 100% **C**$^{\cdot+}$ solution.*

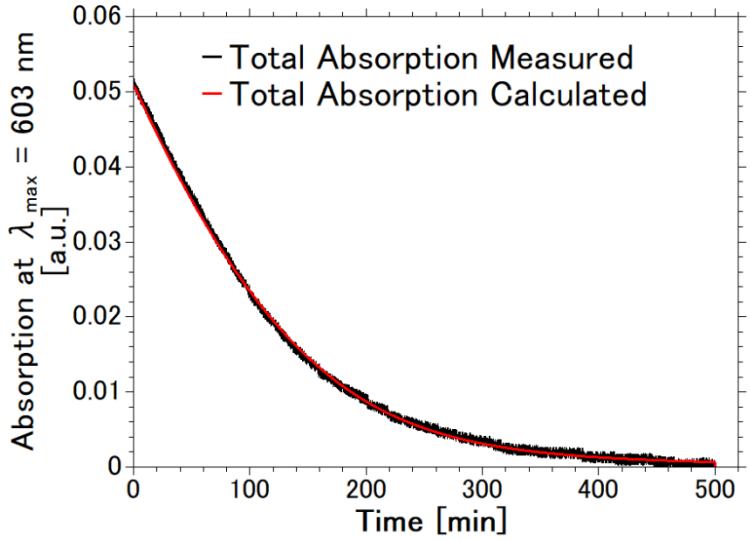

*Figure S16. Experimental (black) and calculated thermal decays at λ_{max} of a PSS solution of **4** in acetonitrile showing the optimised kinetic fitting.*

References

[1] Frisch, M. J.; Trucks, G.W.; Schlegel, H. B.; Scuseria, G. E.; Robb, M. A.; Cheeseman, J. R.; Scalmani, G.; Barone, V.; Mennucci, B.; Petersson, G. A.; Nakatsuji, H.; Caricato, M.; Li, X.; Hratchian, H. P.; Izmaylov, A. F.; Bloino, J.; Zheng, G.; Sonnenberg, J. L.; Hada, M.; Ehara, M.; Toyota, K.; Fukuda, R.; Hasegawa, J.; Ishida, M.; Nakajima, T.; Honda, Y.; Kitao, O.; Nakai, H.; Vreven, T.; Montgomery Jr, J. A.; Peralta, J. E.; Ogliaro, F.; Bearpark, M.; Heyd, J. J.; Brothers, E.; Kudin, K. N.; Staroverov, V. N.; Kobayashi, R.; Normand, J.; Raghavachari, K.; Rendell, A.; Burant, J. C.; Iyengar, S. S.; Tomasi, J.; Cossi, M.; Rega, N.; Millam, J. M.; Klene, M.; Knox, J. E.; Cross, J. B.; Bakken, V.; Adamo, C.; Jaramillo, J.; Gomperts, R.; Stratmann, R. E.; Yazyev, O.; Austin, A. J.; Cammi, R.; Pomelli, C.; Ochterski, J. W.; Martin, R. L.; Morokuma, K.; Zakrzewski, V. G.; Voth, G. A.; Salvador, P.; Dannenberg, J. J.; Dapprich, S.; Daniels, A. D.; Farkas, Ö.; Foresman, J. B.; Ortiz, J. V.; Cioslowski, J.; Fox, D. J. Gaussian 09 Revision A.02, Gaussian Inc. Wallingford CT, 2009.

[2] T. Nakashima, K. Atsumi, S. Kawai, T. Nakagawa, Y. Hasegawa and T. Kawai, *Eur. J. Org. Chem.*, 2007, **19**, 3212-3218.

[3] Kawai, Tsuyoshi; et al Patent, Japan, JP2018140974 A 2018-09-13

[4] R. Asato, C. Martin, J. Calupitan, R. Mizutsu, T. Nakashima, G. Okada, N. Kawaguchi, T. Yanagida and T. Kawai, *Chem. Sci.*, 2020, **11**, 2504-2510.